

1 **The protein phosphatase PPKL is a key regulator of daughter parasite**
2 **development in *Toxoplasma gondii***

3 Chunlin Yang¹, Emma H. Doud^{2,3,4}, Emily Sampson¹, Gustavo Arrizabalaga^{1,5#}

4 ¹Department of Pharmacology and Toxicology,

5 ²Department of Biochemistry and Molecular Biology,

6 ³Center for Proteome Analysis,

7 ⁴Melvin and Bren Simon Comprehensive Cancer Center,

8 ⁵Department of Microbiology and Immunology,

9 Indiana University School of Medicine, Indianapolis, Indiana, USA.

10

11 Running Head: PPKL regulates *Toxoplasma* daughter development.

12

13 # Address correspondence to Gustavo Arrizabalaga, garrizab@iu.edu.

14

15 **Abstract**

16 Apicomplexan parasites, including *Toxoplasma gondii*, encode many plant-like proteins,
17 which play significant roles and present attractive targets for drug development. In this study, we
18 have characterized the plant-like protein phosphatase PPKL, which is unique to the parasite and
19 absent in its mammalian host. We have shown that its localization changes as the parasite
20 divides. In non-dividing parasites, it is present in the cytoplasm, nucleus, and pre-conoidal region.
21 As the parasite begins division, PPKL is enriched in the pre-conoidal region and the cortical
22 cytoskeleton of the nascent parasites. Later in the division, PPKL is present in the basal
23 complex ring. Conditional knockdown of PPKL showed that it is essential for parasite
24 propagation. Moreover, parasites lacking PPKL exhibit uncoupling of division, with normal DNA
25 duplication but severe defects in forming daughter parasites. While PPKL depletion does not
26 impair the duplication of centrosomes, it affects the rigidity and arrangement of the cortical
27 microtubules. Both Co-Immunoprecipitation and proximity labeling identified the kinase DYRK1
28 as a potential functional partner of PPKL. Complete knockout of *DYRK1* phenocopies lack of
29 PPKL, strongly suggesting a functional relationship between these two signaling proteins.
30 Global phosphoproteomics analysis revealed a significant increase in phosphorylation of the
31 microtubule-associated proteins SPM1 in PPKL-depleted parasites, suggesting PPKL regulates
32 the cortical microtubules by mediating the phosphorylation state of SPM1. More importantly, the
33 phosphorylation of cell cycle-associated kinase Crk1, a known regulator of daughter cell
34 assembly, is altered in PPKL-depleted parasites. Thus, we propose that PPKL regulates
35 daughter parasite development by influencing the Crk1-dependent signaling pathway.

36 **Importance**

37 *Toxoplasma gondii* can cause severe disease in immunocompromised or immunosuppressed
38 patients and during congenital infections. Treating toxoplasmosis presents enormous
39 challenges since the parasite shares many biological processes with its mammalian hosts,
40 which results in significant side effects with current therapies. Consequently, proteins that are
41 essential and unique to the parasite represent favorable targets for drug development.
42 Interestingly, *Toxoplasma*, like other members of the phylum Apicomplexa, has numerous plant-
43 like proteins, many of which play crucial roles and do not have equivalents in the mammalian
44 host. In this study, we found that the plant-like protein phosphatase, PPKL, appears to be a key
45 regulator of daughter parasite development. With the depletion of PPKL, the parasite shows
46 severe defects in forming daughter parasites. This study provides novel insights into the
47 understanding of parasite division and offers a new potential target for the development of
48 antiparasitic drugs.

49 **Keywords**

50 *Toxoplasma, Phosphatase, PPKL, DYRK1, SPM1, Crk1, Division, Cell cycle, phosphorylation*

51 Introduction

52 Apicomplexa phylum species are parasites of humans and other animals, causing various
53 diseases such as malaria, toxoplasmosis, and cryptosporidiosis. Apicomplexa has highly
54 specialized organelles such as micronemes, rhoptries, and polar rings, which are critical in the
55 propagation and virulence of these parasites [1]. Among these unique organelles is the non-
56 photosynthetic plastid known as the apicoplast, which is thought to have originated from an
57 algal endosymbiont engulfed by a common ancestor of the current apicomplexans [2]. This
58 secondary endosymbiotic event is also thought to have resulted in significant horizontal gene
59 transfer from the endosymbiont to the nuclear genome during evolution [2]. As a result,
60 apicomplexan genomes retain a multitude of plant-like genes. Many of these plant-like genes
61 encode unique proteins essential for parasite biology, including the ApiAP2 transcription factors,
62 which are key regulators for apicomplexan life cycle progression and differentiation [3], and the
63 calcium-dependent protein kinases that regulate motility, invasion, and egress [4-7]. As no
64 homologs of most of these plant-like proteins are present in mammalian cells, they serve as
65 favorable drug targets for the development of antiparasitic drugs.

66 The PPP family protein phosphatase PPKL, which contains a Kelch domain at its N-terminal
67 region, is found in land plants and green algae, and, interestingly, in alveolates, including
68 apicomplexans [8]. All available apicomplexan genomes encode a single PPKL [8]. By contrast,
69 *Arabidopsis* encodes four PPKLs, including brassinosteroid-insensitive1 (BRI1) suppressor
70 (BSU1) and BSU-LIKE 1, 2, and 3 (BSL1,2,3) [9]. BSU1 is the most well-studied PPKL and is
71 central to the brassinosteroid signaling pathway in *Arabidopsis* [10, 11]. Brassinosteroids (BRs)
72 are essential growth-promoting hormones in plants, which are ligands of BRI1, a receptor
73 kinase located in the plasma membrane [12, 13]. BRI1 works in conjunction with the co-receptor
74 BRI1-associated kinase 1 (BAK1) [14]. In the absence of BRs, BRI1 is inactive and bound to the
75 inhibitor protein BRI1 kinase inhibitor1 (BKI1) [15]. When BR binds to the extracellular domains

76 of BRI1 and BAK1, the cytoplasmic kinase domain of BRI1 is activated and phosphorylates
77 BKI1, leading to its dissociation [16, 17]. BRI1 is then fully activated by the formation of a
78 heterodimeric complex with BAK1 and phosphorylation of the cytoplasmic domains of both
79 kinases [16, 17]. Activated BRI1 initiates a signaling cascade that leads to the activation of
80 BSU1 by phosphorylation [18, 19]. Activated BSU1 then dephosphorylates BIN2, a plant
81 homolog of glycogen synthase kinase3 (GSK3)-like serine/threonine kinase, which leads to its
82 degradation [19, 20]. In the absence of brassinosteroid, phosphorylated and active BIN2
83 phosphorylates two transcriptional factors, BZR1 (Brassinazole-resistant1) and BES1 (bri1-EMS
84 suppressor1), leading to their retention in the cytoplasm and proteasomal degradation mediated
85 by ubiquitination [21-23]. Thus, dephosphorylation of BIN2 by BSU1 leads to its degradation,
86 which allows BZR1 and BES1 to act in the nucleus to activate the expression of BR-responsive
87 genes [16, 24].

88 While apicomplexans do not produce BRs and lack the receptors and most of the proteins
89 involved in brassinosteroid signaling, they express PPKLs with strong homology to BSU1. To
90 date, the study of PPKL in apicomplexans has been limited to *Plasmodium*, where it was found
91 to be dominantly expressed in female gametocytes and ookinetes, and deletion of PfPPKL
92 resulted in defects in the integrity of apical structures, motility, and mosquito invasion [25]. To
93 further explore the function of PPKL in apicomplexans, we have focused on PPKL in
94 *Toxoplasma gondii*, an obligate intracellular parasite in the phylum Apicomplexa. *Toxoplasma*
95 infection is prevalent in humans worldwide. Although *Toxoplasma* infection poses a minimal
96 danger to people with healthy immune systems, it constitutes a considerable threat to
97 immunocompromised patients and during congenital infections [26, 27]. The available drugs that
98 can treat toxoplasmosis are very limited and have significant toxic side effects [28]. Here we
99 show that PPKL has a highly dynamic localization pattern during parasite division and that,
100 importantly, it is essential for parasite division. Moreover, we show that PPKL is an important

101 part of the signaling pathways that control cell cycle, division, and cytoskeletal regulation.
102 Therefore, this work sheds light on the unique processes by which this important pathogen
103 divides and reveals an essential enzyme that could serve as a target for much-needed
104 therapeutics.

105 **Results**

106 **PPKL exhibits multiple cellular localizations and is associated with the progression of**
107 **daughter parasite formation.**

108 PPKL in *Toxoplasma* consists of a sequence of 934 amino acids, which exhibits a structural
109 organization like its homolog in plants and other apicomplexans, featuring six kelch motifs
110 located in the N-terminal region, followed by the protein phosphatase domain situated in the C-
111 terminal region (Fig. 1A). To determine where PPKL localizes within the parasite, we used a
112 CRISPR/Cas9-based strategy to generate a strain in which the endogenous gene encoded a C-
113 terminal triple hemagglutinin (3xHA) epitope tag. The resulting strain, $\Delta ku80$:PPKL.3xHA
114 (referred to as PPKL^{HA} hereafter), was used for immunofluorescence assays (IFA) of
115 intracellular parasites. As transcriptomic data shows that *PPKL*'s expression varies during the
116 cell cycle (ToxoDB), we co-stained parasites for the inner membrane complex (IMC) protein
117 IMC3 to monitor parasite division and daughter cell formation. In non-dividing parasites, PPKL is
118 present throughout the parasite and can be detected in both the cytoplasm and the nucleus (Fig.
119 1B). To confirm that PPKL is present in the nucleus, we performed cytoplasmic and nuclear
120 fractionation of PPKL^{HA} parasites and then compared the ratio of PPKL in the nuclear fraction
121 with that of the exclusively cytoplasmic protein eIF2 α [29]. The results showed that PPKL was
122 significantly enriched in the nuclear fraction in relation to eIF2 α (Fig. S1).

123 Interestingly, in dividing parasites, PPKL appears to be associated with the daughter
124 parasites and is enriched in the cortical cytoskeleton of the daughter parasites (Fig. 1C and D).
125 Intriguingly, we found that in a small fraction (6.5% \pm 0.7%) of parasites, PPKL was heavily
126 enriched in two distinct bright spots, which partially overlapped with the two duplicated
127 centrosomes labeled by the anti-centrin1 antibody (Figure 1E). This localization suggests that
128 PPKL may be present in the daughter parasite buds at a very early stage of division before the
129 formation of IMC of the daughter cells (Fig. 1E).

130 For a more detailed analysis of PPKL localization, we performed Ultrastructure Expansion
131 Microscopy (U-ExM) [30, 31]. To observe the protein and other parasite features of interest, we
132 employed NHS-ester to stain all proteins, an acetylated-tubulin antibody to visualize
133 microtubules, an anti-HA antibody to detect HA-tagged PPKL, and Draq5 to label DNA. As we
134 have seen by standard IFA, analysis of U-ExM images of parasites that have expanded in
135 volume by approximately 100-fold corroborate that PPKL is present throughout the parasite in
136 non-dividing ones and appeared to enrich in the cortical cytoskeleton of daughter parasites (Fig.
137 2A, 2B). Interestingly, U-ExM allowed us to observe that PPKL is enriched at the apical end of
138 both mother and daughter parasites in a ring-like pattern (Fig. 2A, 2B). To more clearly
139 determine whether the PPKL ring overlapped with the apical polar ring or the preconoidal region,
140 we performed U-ExM for extracellular parasites to observe parasites with extended conoids. In
141 extracellular parasites with protruded conoid, the PPKL ring was on the apical end of the conoid
142 (Fig. 2C, 2D), suggesting that PPKL is present in or near the preconoidal region. Remarkably,
143 we observed that during the earliest stages of division, PPKL is one of the earliest components
144 present in the daughter parasite scaffold (Fig. 2E), which only contained two rings, one labeled
145 by PPKL, and a second one, presumably the apical polar ring, labeled by anti-acetylated tubulin
146 antibody. In addition, we observed that in daughter parasites late in the division, PPKL was
147 enriched in the basal complex ring (Fig. 2F), suggesting that PPKL may be involved in
148 terminating the extension of microtubules or in the contraction of the basal complex ring. In sum,
149 both IFA and U-ExM showed that PPKL is present in multiple cellular locations and that the
150 dynamic localization pattern is associated with the progression of daughter parasite formation,
151 suggesting that PPKL may play multiple roles during daughter parasite development.

152 **Depletion of PPKL in parasites leads to disruption of parasite division.**

153 Through a *Toxoplasma* genome-wide CRISPR screen, PPKL was assigned a fitness score
154 of -5.02 [32], suggesting that it is essential for parasite survival and, therefore, that knockout of

155 the *PPKL* gene is not likely possible. Accordingly, to investigate its function, we generated a
156 conditional knockdown strain by using the auxin-induced degradation (AID) system [33]. For this
157 purpose, we inserted an AID-3xHA prior to the stop codon of the endogenous *PPKL* gene using
158 CRISPR-mediated gene editing. Western blot of the resulting PPKL^{AID-HA} strain showed that
159 treatment with auxin significantly reduced the amount of PPKL within half an hour and almost
160 completely depleted PPKL within one hour (Fig. 3A). To determine if PPKL is required for
161 *Toxoplasma* propagation, we performed plaque assays of both the parental and PPKL^{AID-HA}
162 strains with and without auxin. Consistent with the low fitness score, PPKL^{AID-HA} parasites
163 treated with auxin failed to form any plaques (Fig. 3B and C), indicating that PPKL is essential
164 for parasite propagation. In addition, we observed that untreated PPKL^{AID-HA} parasites formed
165 fewer and smaller plaques than the parental strain (Fig. 3B and C), which may be due to the
166 significantly lower expression of PPKL-AID in relation to the parental strain (Fig. S2) or perhaps
167 because the fusion of AID to PPKL may slightly impair its function.

168 To determine the cellular consequences of PPKL depletion, we performed IFA to observe
169 the morphology of PPKL^{AID-HA} parasites treated with auxin. Briefly, we added auxin to the culture
170 2 hours after infection and allowed parasites to grow overnight (~18h). IFAs were performed
171 using antibodies against acetylated tubulin and IMC3 to monitor the formation of daughter cells.
172 Strikingly, in the auxin-treated PPKL^{AID-HA} cultures, most vacuoles contained only one extremely
173 swollen parasite, whereas untreated vacuoles mostly had 4 to 8 parasites (Fig. 3D).
174 Interestingly, these swollen parasites contained a large amount of DNA, far exceeding the
175 amount of a normal single parasite (Fig. 3D and E). However, most (71% ± 6%) of these
176 swollen parasites did not have any daughter parasites (Fig. 3E, top row), and only a few (10% ±
177 2%) contained a varied number of seemingly abnormal daughter parasites (Fig. 3E, middle row).
178 Moreover, there were some (18% ± 4%) vacuoles containing two expanded parasites, similarly
179 with an increased amount of DNA (Fig. 3E, bottom row). When we extended the treatment of

180 auxin to two days (~42h), the vacuoles became more disorganized, had more abnormal
181 parasites, and swollen parasites had a further accumulation of DNA (Fig. 3F), implying that
182 division was progressing, albeit abnormally. In summary, PPKL-depleted parasites have
183 deficiencies in daughter parasite formation. Still, their ability to replicate DNA appears relatively
184 unimpaired, resulting in severe division uncoupling.

185 **Depletion of PPKL does not affect the replication of centrosomes.**

186 During endodyogeny, the two daughter parasite scaffolds are assembled near the two
187 centrosomes in a one-to-one correspondence [34]. Centrosome duplication has been shown to
188 occur before the formation of the daughter parasites, and it is needed for the division to initiate
189 [35, 36]. Based on the significant defects in parasite division in the PPKL mutant, we monitored
190 centrosome duplication upon PPKL depletion. As expected, untreated dividing parasites had
191 exactly two centrosomes in each mother cell (Fig. 4A). Similarly, parasites treated with auxin
192 overnight had at least two centrosomes (Fig. 4A), regardless of whether they contained
193 daughter parasites or not, implying that centrosome duplication was still taking place.
194 Interestingly, we often observe treated parasites with more than two centrosomes (Fig. 4A). It
195 should be considered that, under normal conditions, parasites that have been cultured overnight
196 would have undergone two to three divisions. Thus, the presence of more than two
197 centrosomes within one parasite is consistent with our observation that PPKL depletion leads to
198 division (i.e., centrosome and DNA duplication) and daughter parasite formation being
199 uncoupled.

200 To further examine centrosome duplication in PPKL-depleted parasites, we added auxin
201 right after infection and allowed the parasites to grow for six hours, which allowed us to monitor
202 the first division cycle of the parasites after PPKL depletion. IFA showed that few parasites had
203 detectable daughter parasites for both the control and auxin treated. Interestingly, among the
204 parasites that were dividing, 85%±1.5% of those from auxin-treated parasites had only one

205 daughter parasite (Fig. 4B and C). $95\% \pm 1.5\%$ of the parasites containing only one daughter had
206 two centrosomes. We also observed that in the treated parasites, the single-daughter parasite
207 appeared to be morphologically unusual and larger than normal. We explored this phenotype
208 using U-ExM and observed that the microtubule system of the single daughter parasite
209 appeared to be normal, except that the gaps between the cortical microtubules were wider,
210 which correlates with the larger appearance of the parasites (Fig. 4D). As shown in Fig. 4D, we
211 also observed parasites in which there were two centrosomes and two spindles, with only one of
212 the spindles associated with the DNA. Taken together, our results suggest that although division
213 is impaired upon depletion of PPKL, centrosome duplication remains unaffected.

214 **Depletion of PPKL reduces the rigidity of microtubules.**

215 A previous study has shown that the knockout of the PPKL gene in *Plasmodium* led to
216 apical microtubule disorganization and dissociation from the IMC [25]. Interestingly, PPKL also
217 appears to be required to maintain the order and/or rigidity of microtubules in *Toxoplasma*, as
218 observed through the disruption of the compact structure of the cortical cytoskeleton in the
219 knockdown strain. To confirm this observation, we treated PPKL^{AID-HA} parasites that had
220 undergone two to three rounds of division with auxin for six hours and isolated their cortical
221 cytoskeleton using sodium deoxycholate. As expected, the cortical cytoskeleton from the control
222 parasites appeared more compact with few fragmented microtubules (Fig. 5A). By contrast, the
223 cortical cytoskeleton from auxin-treated parasites appeared more disordered with five times
224 more fragmented microtubules than the control (Fig. 5A, B), suggesting that PPKL is involved in
225 the regulation of the rigidity and compact structure of the cortical microtubule system.

226 **IMC29 and DYRK1 are likely PPKL functional partners.**

227 To determine the molecular mechanisms responsible for the PPKL knockdown phenotypes,
228 we set out to identify functional partners and putative substrates of PPKL. We first performed
229 standard co-immunoprecipitation (Co-IP) using anti-HA conjugated magnetic beads to

230 precipitate HA-tagged PPKL from the PPKL^{HA} parasites. However, this approach failed to
231 identify PPKL interactors, suggesting that either PPKL works on its own or that it interacts with
232 other proteins and substrates transiently or with low affinity. Accordingly, we used disuccinimidyl
233 sulfoxide (DSSO) to crosslink the protein samples before performing Co-IP. The results of the
234 tandem mass spectrometry (MS/MS) analysis indicated that two proteins significantly co-
235 precipitated with PPKL: IMC29 (TGGT1_243200) and DYRK1 (TGGT1_204280)
236 (Supplementary Dataset 1). The inner membrane IMC29 has been identified as a crucial
237 component of the early daughter buds with a substantial contribution to parasite division [26].
238 DYRK1 is a cell-cycle-related protein kinase of unknown function.

239 As a complementary approach to the Co-IP, we used the TurboID proximity labeling method
240 [37], which can identify neighboring and interacting proteins, including substrates. To this end,
241 we endogenously fused the engineered biotin ligase TurboID and a 3xHA epitope tag to the C-
242 terminus of PPKL. IFA of the obtained parasite strain showed that PPKL^{TurboID.HA} has the same
243 localization pattern as PPKL^{HA} (Fig. S3A). We then confirmed that the fusion was active by
244 incubating the PPKL^{TurboID.HA} parasites with D-biotin and performed western blot, which showed
245 a significant increase in biotinylated proteins compared to the same parasite strain without biotin
246 treatment (Fig. S3B). To identify interacting and neighboring proteins, we incubated
247 PPKL^{TurboID.HA} or parental strain parasites with D-biotin and isolated biotinylated proteins for
248 MS/MS for two experimental replicates. We applied the following criteria to the resulting list of
249 putative interactors: 1) a total of 10 or more between the two replicates, and 2) an experiment to
250 control fold change equal to or larger than 3.5. In this manner, we obtained a list of 81 putative
251 PPKL neighboring and/or interacting proteins (Table 1 and Supplementary Dataset 2). To
252 further analyze this list of proteins, we investigated their potential molecular functions based on
253 functional annotations on ToxoDB. Out of the 81 proteins, 19 are related to the cortical
254 cytoskeleton system, including the IMC, the apical complex, the basal complex, and

255 microtubules; 7 are potentially related to vesicle transport; 5 are potentially related to RNA
256 splicing (Table 1). Moreover, there are three protein kinases (TGGT1_231070, DYRK1, and
257 SRPK1) and one protein phosphatase, PPM2A. Notably, both IMC29 and DYRK1, which were
258 identified as putative interactors via crosslinking and IP, were identified with the TurboID
259 approach, suggesting that they are highly likely functional partners of PPKL.

260 **DYRK1 plays an important role in the *Toxoplasma* division.**

261 Based on the division phenotype of PPKL-depleted parasites, it is likely that PPKL
262 participates in a signaling pathway that regulates parasite division. As signaling pathways often
263 involve a chain of kinases and phosphatases, we focused on characterizing the function of
264 DYRK1, which appears to be a putative PPKL interactor. Dual-specificity tyrosine-regulated
265 kinase (DYRK) is a member of the CMGC group of kinases [38], a large and conserved family of
266 kinases that play key roles in cell cycle regulation and many important signaling pathways [39].
267 *Toxoplasma* encodes two DYRKs in its genome, and phylogenetic analysis (Fig. 6A), including
268 human and Arabidopsis homologs, showed that DYRK1 was exclusively clustered with the plant
269 homologs, while DYRK2 (TGGT1_283480) was clustered with human homologs. Thus, both
270 PPKL and DYRK1 are closer in homology to proteins from plants. To identify the localization of
271 DYRK1, we endogenously fused a 3xMyc ectopic tag at its C-terminus with CRISPR/Cas9
272 mediated gene editing. IFA showed that in non-dividing parasites, DYRK1 localizes to the
273 nucleus (Fig. 6B top row); while in parasites undergoing division, it exclusively localizes to the
274 IMCs of daughter parasite buds (Fig. 6B bottom row). The dynamic localization of DYRK1
275 suggests that this kinase might have multiple roles throughout the division cycle of the parasite.

276 As a potential functional partner of PPKL, we sought to investigate whether the absence of
277 DYRK1 manifests phenotypic similarities to the PPKL knockdown. For this purpose, the *DYRK1*
278 gene was disrupted through the replacement of the coding region with a DHFR expression
279 cassette in the parental $\Delta ku80$ parasites by using the CRISPR/Cas9 system (Fig. 6C). The

280 disruption of the *DYRK1* locus in the resulting Δ *DYRK1* strain was confirmed by PCR with four
281 sets of primers (Fig. 6D). Plaque assay showed that Δ *DYRK1* parasites are less efficient at
282 forming plaques as compared to the parental strain (40 ± 15 % plaquing efficiency relative to
283 parental, Fig. 6E, F). While these data suggest that *DYRK1* is not essential, it appears to play
284 an important role in parasite propagation. Importantly, IFA revealed that $53.5\% \pm 6.5\%$ of
285 vacuoles formed by Δ *DYRK1* parasites displayed abnormal parasite division (Fig. 6G, H),
286 characterized by predominantly unsynchronized division, resulting in disorganized parasites
287 within the vacuole and even atypical morphologies for some parasites, such as swollen
288 parasites similar to what is observed upon PPKL depletion. The observed division defect,
289 stemming from the deletion of *DYRK1*, strongly indicates the significant involvement of *DYRK1*
290 in regulating parasite division and a potential functional relationship between PPKL and *DYRK1*.

291 **PPKL influences the phosphorylation state of regulators of microtubule rigidity and cell**
292 **division.**

293 To further explore the molecular mechanisms leading to the division phenotypes of PPKL-
294 depleted parasites, we used tandem mass tag (TMT) quantitative mass spectrometry to
295 compare the phosphoproteomes of PPKL^{AID} parasites treated with/without auxin. Briefly,
296 PPKL^{AID-HA} parasites were allowed to grow for 18 hours before adding either auxin or ethanol
297 (vehicle control). After one, three, and six hours of treatment, cultures were harvested, and the
298 parasites were released by syringe lysis, and samples were prepared for quantitative mass-
299 spectrometry. At the 6-hour timepoint, we identified 486 phosphopeptides from 313 proteins that
300 were more than 2-fold abundant in the auxin-treated parasites (Fig. 7A, Supplementary dataset
301 3). We also identified 425 phosphopeptides from 255 proteins that were more than 2-fold less
302 abundant upon PPKL depletion (Fig. 7A, Supplementary dataset 3). Interestingly, 86 proteins
303 had both over and under-phosphorylated peptides. Thus, we identified a total of 482 proteins
304 whose phosphorylation state was PPKL-dependent. Interestingly, 24 of the 81 proteins identified

305 in the TurboID assay were among these 482 proteins (Supplementary Dataset 3), strongly
306 validating the reliability of the phosphoproteome and interactome data. However, DYRK1 was
307 not among these 24 proteins, and it had a 1.22-fold increase in phosphorylation of one residue
308 and a 1.16-fold decrease in phosphorylation of another upon depletion of PPKL.

309 As expected, the results from the parasites treated for either one or three hours revealed a
310 more limited number of peptides exhibiting PPKL-dependent phosphorylation status, especially
311 for the 1-hour treated samples (Supplementary Dataset 4). Therefore, when filtering the
312 quantitative proteomic data, we followed the 2-fold change as the cutoff for 3-hour timepoint
313 samples but reduced the fold change from 2 to 1.5 for the 1-hour timepoint samples to prevent
314 missing important information. Thus, we identified 204 proteins (over: 124 peptides from 101
315 proteins; under: 153 peptides from 123 proteins; both: 20 proteins) that exhibited PPKL-
316 dependent phosphorylation state in the 3-hour timepoint samples, and 304 proteins (over: 142
317 peptides from 124 proteins, under: 278 peptides from 212 proteins; both: 32 proteins) in the 1-
318 hour timepoint samples (Fig. 7A, Supplemental Dataset 4). When combining the data to identify
319 phosphopeptides shared by all three time points samples, we found 13 phosphopeptides from
320 11 proteins were over-phosphorylated, and 22 phosphopeptides from 19 proteins were under-
321 phosphorylated (Table 2, Fig. 7B). One of these proteins, TGGT1_214270, had both over- and
322 under-phosphorylated peptides identified. Thus, we obtained a list of 29 proteins whose
323 phosphorylation was affected by lack of PPKL at all three time points of auxin treatment (Table
324 2).

325 Interestingly, among these 29 proteins, two were identified as putative interactors and/or
326 substrates of PPKL via TurboID: SPM1 (TGGT1_263520) and TGGT1_204160 (Fig. 7B,
327 Highlighted in Table 2). SPM1, a protein that stabilizes cortical microtubules in *Toxoplasma* [40,
328 41], exhibited a phosphorylation increase of greater than two-fold on either S14 alone or both
329 S14 and S18 in all three timepoint sample sets. TGGT1_204160, an eIF2 α homolog containing

330 a GYF domain, showed decreased phosphorylation upon PPKL depletion. Remarkably, S1326
331 of the cell cycle-related kinase Crk1 (TGGT1_304970) showed a significant decrease in
332 phosphorylation at all three time points (Fig. 7B, Highlighted in Table 2). Crk1 has been shown
333 to play an essential role in daughter parasite assembly [42]. Thus, it is plausible that the
334 decreased phosphorylation of S1326 in Crk1 in the absence of PPKL may contribute to the
335 severe defect in the formation of daughter parasites in PPKL-depleted parasites.

336

337 **Discussion**

338 In this study, we conducted a comprehensive investigation into the localization and function
339 of PPKL in *Toxoplasma*. Our findings demonstrated that PPKL's localization is closely
340 associated with the formation of daughter parasites and that depletion of PPKL has a profound
341 impact on the initiation and development of daughter parasites, highlighting the critical
342 regulatory role of PPKL throughout the process of daughter parasite formation.

343 *Toxoplasma* adopts a unique division process called endodyogeny, where two daughter
344 parasites are generated within the mother cell [34]. The assembly of daughter parasites initiates
345 during the late S-phase of the cell cycle [34, 43]. Each daughter cell is assembled around a
346 centrosome that has already completed the replication process during the early S-phase [34,
347 43]. The exact composition of the initially assembled daughter parasites is unclear, while it is
348 evident that daughter parasites assemble from the apical to the basal end [34, 43]. Previous
349 studies have identified several IMC proteins, such as IMC15, IMC29, and IMC32, which are
350 present early in the nascent daughter parasites [26, 44, 45]. Additionally, the apical cap proteins
351 ISP1, FBX01, and the AC9-AC10-ERK7 complex, were also identified as the earliest
352 components of daughter parasites [46-48]. However, these previous studies relied on traditional
353 IFA to identify the localization of these proteins, which has limitations in detecting daughter
354 parasites at a very early stage, specifically before the assembly of the IMC. Fortunately, by
355 utilizing U-ExM, we were able to observe newly initiated daughter parasites comprising only two
356 rings: a potentially preconoidal ring labeled by PPKL and a presumed apical polar ring labeled
357 by anti-acetylated tubulin antibody (Fig. 2E). This discovery suggests that PPKL appears in
358 daughter parasites earlier than all the early proteins identified thus far and that the structures of
359 the daughter parasite bud that were first assembled were probably the preconoidal region and
360 the apical polar ring.

361 The mechanism which regulates the initiation of daughter parasite assembly also remains
362 enigmatic. One of the prominent phenotypes observed upon PPKL depletion in our study was a
363 significant impairment in the initiation of daughter parasites. After an 18-hour culture period, a
364 substantial portion of PPKL-deficient parasites failed to develop detectable daughter parasites.
365 Furthermore, when PPKL-depleted parasites were subjected to a brief 6-hour treatment with
366 IAA, most of the dividing parasites exhibited only a single daughter parasite. These findings
367 indicate that the absence of PPKL disrupts the regulatory pathway responsible for initiating
368 daughter parasite formation. Previous studies have highlighted the requirement of centrosome
369 replication for proper cell division in *Toxoplasma*, with NEK1 and MAPKL identified as protein
370 kinases involved in regulating centrosome duplication [35, 36]. Surprisingly, our investigation
371 revealed that centrosome duplication remained unaffected in PPKL-depleted parasites.
372 Additionally, our phosphoproteomics analysis did not indicate any impact of PPKL depletion on
373 the phosphorylation status of NEK1 and MAPKL. These findings indicate that PPKL potentially
374 participates in a distinct pathway, separate from the one responsible for regulating centrosome
375 replication associated with NEK1 and MAPKL.

376 Interestingly, our phosphoproteomics analysis revealed that the depletion of PPKL promptly
377 leads to a reduction in the phosphorylation level of Crk1 at S1326, strongly suggesting that
378 PPKL plays a role in regulating the phosphorylation state of S1326 in Crk1. In *Toxoplasma*,
379 Crk1 is an essential cell cycle-associated kinase that partners with the cyclin protein CycL [42].
380 Although the functional role of the Crk1-CycL complex is not well understood, conditional
381 knockdown of Crk1 results in abnormal assembly of the daughter parasite cytoskeleton [42],
382 suggesting that it is involved in regulating the assembly of the daughter parasite scaffold. In
383 mammals, most cyclin-dependent kinases (CDKs) are known to be activated in a two-step
384 process with the binding of a specific cyclin and the phosphorylation of the activation loop (T-
385 loop) in the kinase domain, typically at a conserved threonine residue [49]. Although the T-loop

386 is present in Crk1, no phosphorylation of this conserved threonine has been reported based on
387 available post-translational modification data of Crk1 (ToxoDB). Notably, S1326, which is ~30
388 aa away from the kinase domain, represents the sole identified phosphorylation site within the
389 C-terminal region, encompassing the entire kinase domain (aa 993-1292) and the C-terminal
390 extension (aa 1293-1373), indicating it may be a critical residue for regulating the activity of the
391 kinase domain.

392 Given that PPKL is a phosphatase and the effect on Crk1 S1326 in its absence is a
393 reduction in phosphorylation, the relation between PPKL and Crk1 is unlikely to be a direct one.
394 The plausibly simplest model is that PPKL activates a kinase that subsequently phosphorylates
395 Crk1. The kinase DYRK1, which we identified as physically interacting with PPKL, could be
396 considered a candidate for such a role. Interestingly, the knockout of DYRK1 in our study
397 causes significantly unsynchronized division of the parasites, highlighting its critical role in
398 regulating parasite division. However, the phosphorylation state of DYRK1 does not have
399 notable alteration (1.23-fold change in 6h samples) with the depletion of PPKL. An alternative
400 model for the functional relation between PPKL and Crk1 is that the phosphorylation of S1326 is
401 the result of autophosphorylation. Under such a model, PPKL would dephosphorylate Crk1
402 activating its kinase domain and resulting in Crk1 autophosphorylation. Nonetheless, we did not
403 identify Crk1 as a near neighbor of PPKL. Overall, further investigations are necessary to
404 elucidate the precise mechanism of the functional relationship between PPKL and Crk1.

405 Besides the defect in daughter cell assembly, loss of PPKL resulted in structural changes to
406 cortical microtubules. This finding is consistent with a previous study conducted on *Plasmodium*,
407 which demonstrated that the deletion of PPKL in the parasite led to the dissociation of apical
408 microtubules from the IMC [25]. The cortical microtubules play a crucial role in maintaining the
409 shape and stability of the parasite [41]. The normal cortical microtubule architecture of
410 *Toxoplasma* has robust rigidity and can withstand strong detergent extraction [41]. Our

411 experiments using sodium deoxycholate revealed that PPKL-depleted parasites have more
412 fragile microtubules, suggesting that PPKL is associated with the regulation of the rigidity of
413 cortical microtubules. Along with the loss of rigidity, the cortical microtubules of PPKL-depleted
414 daughter parasites also lose their compact and ordered structure. In those PPKL-depleted
415 parasites undergoing their first cell division, we found that most of those single abnormal
416 daughter parasites had a round shape with much larger gaps between microtubules. This may
417 not only be because these single-daughter parasites are not spatially restricted in the mother
418 parasites without a sibling but also may be mainly due to the loss of the compact and ordered
419 structure of their cortical microtubules. In addition, we also see many other types of irregularly
420 shaped daughter parasites in PPKL-depleted parasites, further supporting PPKL regulates the
421 ordered structure maintenance of the cortical microtubules.

422 The identification of SPM1 as a putative substrate of PPKL might reveal a mechanism by
423 which PPKL regulates microtubules. SPM1 is a filamentous microtubule inner protein, which
424 binds to α , and β tubulins through the whole length of the microtubule [40, 41]. In addition to
425 SPM1, there are two globular microtubule inner proteins in *Toxoplasma*, TrxL1 and TrxL2,
426 bound to the microtubules [41, 50]. Previous detergent extraction experiments have shown that
427 SPM1 plays a more important role in stabilizing microtubules than both TrxL1 and TrxL2, as
428 microtubules without SPM1 cannot withstand even mild detergent extraction, while microtubules
429 without either TrxL1 or TrxL2 can still withstand strong detergent extraction [41]. Our data
430 suggest that PPKL may regulate the SPM1 by dephosphorylating two residues, S14 and S18.
431 Further studies are needed to verify that changes in the phosphorylation state of these two
432 residues have a significant effect on the stability of the microtubule.

433 PPKL exhibits an intriguing localization pattern in both mother and daughter cells of
434 *Toxoplasma*, specifically in the pre-conoidal region. This localization suggests that PPKL may
435 have an undiscovered role in this particular region. Our ongoing research aims to elucidate the

436 specific function of PPKL in the preconoidal region. Furthermore, we have observed that PPKL
437 localizes to the basal complex ring of daughter parasites during the late stages of division, and
438 the basal complex protein BCC7 is one of its neighboring proteins, indicating a potential
439 functional role of PPKL in the basal complex. However, previous proximity-based biotinylation
440 labeling by multiple basal complex proteins did not identify PPKL [51]. Thus it is likely that PPKL
441 is associated with the microtubule ends but not the basal complex itself. Accordingly, its role
442 there may be related to the termination of the extension of microtubules since, as stated above,
443 we have found that many PPKL-depleted parasites have elongated microtubules that run the full
444 length of the parasite.

445 The closest homolog of PPKL in plants, Bsu1, positively regulates the brassinosteroid
446 signaling pathway through the dephosphorylation of a conserved tyrosine in the CMGC family
447 protein kinase Bin2 [10]. Interestingly, *Toxoplasma* encodes for a Bin2 homolog
448 (TGGT1_265330) that is known to be phosphorylated at the corresponding tyrosine.
449 Nonetheless, we did not identify TgBin2 as either an interactor or a putative substrate in our
450 unbiased approaches. Interestingly, DYRK1, which has been identified as a putative functional
451 partner of PPKL in this study, also belongs to the CMGC kinase family and possesses a
452 phosphorylated tyrosine within a conserved region similar to the phosphorylated tyrosine region
453 of Bin2. This intriguing observation suggests the possibility that PPKL may regulate the activity
454 of DYRK1 by dephosphorylating this conserved tyrosine. Our ongoing research aims to
455 investigate this potential relationship further.

456 All these data taken together provide a picture of the various roles potentially played by
457 PPKL in *Toxoplasma* and allow us to propose a preliminary model (Fig. 8). We propose that
458 PPKL acts as a key regulator of daughter parasite development in *Toxoplasma*. The dynamic
459 localization of PPKL at different stages of the cell cycle would allow it to precisely regulate the
460 formation and development of daughter parasites as division progresses. The regulation of

461 daughter parasite development by PPKL may begin with the regulation of an unknown pathway
462 that activates Crk1. As division begins, PPKL is recruited earliest formed preconoidal region,
463 although the role it plays there is unknown. With the assembly of microtubules, PPKL appears
464 to play a role in maintaining the rigidity and compact structure of the cortical microtubules,
465 probably by dephosphorylation of microtubule-associated proteins SPM1. Interestingly, at the
466 late stage of daughter parasite development, PPKL enriches the basal complex ring. It is not
467 known what role it plays at this stage, but our data suggest that it may regulate the length of the
468 microtubules, as we observed that in many PPKL-depleted parasites, the microtubules
469 extended to the very bottom of the cell (Fig. 3E bottom).

470 Overall, the findings of this study highlight the key role of PPKL, a plant-like protein
471 phosphatase, in governing the development processes of daughter parasites in *Toxoplasma*.
472 While potential functional relationships between PPKL and Crk1, as well as PPKL and SPM1,
473 have been identified, the precise molecular mechanisms underlying PPKL's involvement in the
474 various stages of daughter parasite development remain largely elusive. Further comprehensive
475 investigations into the regulatory mechanisms related to PPKL would greatly contribute to our
476 understanding of the initiation and subsequent development processes of daughter parasites in
477 *Toxoplasma*. Such studies hold great promise in providing exciting prospects for the
478 development of antiparasitic drugs.

479

480 **Materials and Methods**

481 **Parasite cultures**

482 *Toxoplasma* tachyzoites used in this study were maintained in human foreskin fibroblasts
483 (HFF) with standard growth medium as previously described [52]. Wild-type parasites used in
484 this study include the strain RH lacking HXGPRT and Ku80 (RH Δ ku80 Δ hxgp r t, referred to as
485 Δ ku80) [53] and the strain stably expressing the plant auxin receptor transport inhibitor response
486 1 (TIR1) (RH Δ ku80 Δ hxgp r t::TIR1, referred to as TIR1) [33].

487 **Generation of parasite lines**

488 All primers used for molecular cloning and site-directed mutagenesis are listed in
489 Supplemental Dataset 5. To tag endogenous genes with a hemagglutinin (HA) or Myc epitope
490 tag in the C-terminus, we amplified 3xHA/Myc-DHFR/HXGPRT amplicons from the plasmids
491 LIC-3xHA-DHFR/HXGPRT or LIC-3xMyc-DHFR/HXGPRT with primers containing a 5' overhang
492 identical to the sequence immediately upstream of the stop codon, and a 3' overhang identical
493 to the sequence after the Cas9 cutting site. To direct these templates to the desired locus, we
494 generated CRISPR/Cas9 vectors by mutating the UPRT guide RNA sequence in the plasmid
495 pSag1-Cas9-U6-sgUPRT [33] to a guide RNA sequence of the target gene by using Q5 Site-
496 Directed Mutagenesis Kit (NEB). The CRISPR/Cas9 plasmid and the PCR amplicon were
497 transfected into corresponding parental parasites by using the Lonza Nucleofector and
498 Manufacture suggested protocols. Transfected parasites were selected with either
499 pyrimethamine (for selection of DHFR cassette) or MPA/Xanthine (for selection of HXGPRT
500 cassette) and then cloned by limiting dilution as previously described [54].

501 The PPKL conditional knockdown parasite line was generated based on the same
502 CRISPR/Cas9 mediated strategy described above. The amplicon with regions of homology with
503 the PPKL locus was amplified from the plasmid pAID-3xHA-DHFR [33]. The same

504 CRISPR/Cas9 plasmid used for PPKL endogenous 3' tagging was transfected together with the
505 AID-3xHA-DHFR amplicon into the TIR1-expressing parasites [33]. DYRK1 knockout parasite
506 strains were generated based on the CRISPR/Cas9 mediated strategy described previously [54].
507 Briefly, two guide RNA target sites were separately selected in the first exon, and the 3' UTR of
508 the DYRK1 gene and two CRISPR/Cas9 plasmids were generated. The guide RNA expression
509 cassette from one plasmid was amplified and inserted into the KpnI cutting site of the other
510 plasmid to generate a CRISPR/Cas9 plasmid that expresses two guide RNAs. An amplicon of
511 the DHFR selection cassette was co-transfected into $\Delta ku80$ parasites together with the double-
512 guide RNA CRISPR/Cas9 plasmid to bridge the two cut sites via homologous recombination.

513 **Plaque assays**

514 Standard plaque assays were performed as described before [52]. Briefly, 500 parasites of
515 each parasite strain were seeded into host cell monolayers grown in 12-well plates, and cultures
516 were then grown for six days. Cultures were then fixed and stained with crystal violet. Host cell
517 plaques were quantified as previously described [52].

518 **Immunofluorescence assays**

519 Immunofluorescence assays (IFAs) were performed as previously described [52]. The
520 primary antibodies used include rabbit/mouse anti-HA/Myc (Cell Signaling Technology), rabbit
521 anti-IMC6 (1:1000), rabbit anti-Centrin1 (1:1000), rat anti-IMC3 (1:1000), and rabbit/mouse anti-
522 acetylated-Tubulin (1:5000). A Nikon Eclipse E100080i microscope was used for imaging.

523 **Ultrastructure Expansion Microscopy (U-ExM)**

524 Ultrastructure Expansion Microscopy (U-ExM) was performed with intracellular and
525 extracellular parasites as previously described [30, 31]. The antibodies used include rabbit anti-
526 HA (1:500) and anti-Centrin1 (1:500), and mouse anti-acetylated-Tubulin (1:500). The
527 fluorescent antibodies used include Alexa Fluor 405 NHS-Ester (1:250), Alexa Fluor 594 (1:500),

528 488(1:500), and DRAQ5™ Fluorescent Probe (1:250). LSM 800 and 900 microscopes were
529 used for imaging using previously described parameters [31].

530 **Western blots**

531 Western blots were performed as described previously [52]. The primary antibodies used
532 include rabbit anti-HA, anti-eIF2, anti-histone H3, and mouse anti-Sag1. The secondary
533 antibodies utilized were HRP-labeled Anti-Mouse and Anti-Rabbit IgG. The primary antibodies
534 were used at a dilution of 1:5,000, while the secondary antibodies were used at a dilution of
535 1:10,000.

536 **Sodium Deoxycholate extraction**

537 Parasite extraction using Sodium Deoxycholate was conducted following the previously
538 described method [55]. Briefly, PPKL^{AID} parasites were cultured in host cells overnight and
539 subsequently treated with either auxin or ETOH for 6 hours. Intracellular parasites were then
540 released using syringe lysis, and the parasites were deposited onto poly-L-lysine-coated
541 coverslips by centrifugation at 100 g for 1 minute. Subsequently, the parasites were exposed to
542 10 mM Sodium Deoxycholate for 20 minutes at room temperature. Afterward, the parasites
543 were fixed using cold methanol for 8 minutes, followed by IFA utilizing anti-acetylated tubulin
544 and anti-IMC6 antibodies.

545 **Crosslinking and immunoprecipitation**

546 Crosslinking and immunoprecipitation were performed as previously described [54] with
547 some modifications. Briefly, intracellular parasites (PPKL-3xHA or the parental $\Delta ku80$ strain)
548 grown in host cells for 24-28 hours were harvested together with host cells by scrapping in cold
549 PBS. After centrifugation, the pellet was resuspended in PBS supplemented with 5mM DSSO
550 (Thermo Scientific) and incubated at room temperature for 10 minutes. Crosslinking was
551 quenched by adding Tris buffer (1 M, pH 8.0) to a final concentration of 20 mM. After two

552 washes with PBS, the samples were lysed with 1 ml RIPA lysis buffer supplemented with
553 protease and phosphatase inhibitor cocktail (Thermo Scientific) at 4°C for 1h. The lysate was
554 then incubated with mouse IgG magnetic beads overnight at 4°C for pre-clearing and then
555 incubated with mouse anti-HA magnetic beads for 4 hours at 4°C. After washes with RIPA lysis
556 buffer and PBS, the beads were submitted to the Indiana University School of Medicine
557 Proteomics Core facility for liquid chromatography coupled to tandem mass spectrometry
558 (LC/MS-MS) analysis.

559 **Biotinylation by TurboID**

560 PPKL^{TurboID-3xHA} or the control $\Delta ku80$ parasites were cultured in host cells for around 24
561 hours. The medium was supplemented with D-biotin (dissolved in DMSO) to a final
562 concentration of 200 μ M, and cultures were incubated for 3 hours before harvesting by scraping
563 in cold PBS. The samples were washed with cold PBS three times to eliminate biotin. Then the
564 samples were lysed with 1 ml cold RIPA lysis buffer supplemented with 1x protease inhibitor
565 cocktail (Thermo Scientific) and 1mM PMSF for 1h at 4 °C. After centrifugation, the supernatant
566 of the lysate was incubated with DynaBeads MyOne Streptavidin CI beads (Invitrogen) overnight
567 at 4 °C. The beads were washed two times with 1 ml of RIPA lysis buffer, once with 1 ml of 1M
568 KCl, once with 1 ml of 0.1 M Na₂CO₃, and once with 1 ml of 2 M urea in 10 mM Tris-HCl (pH 8.0)
569 and two times with 1ml of RIPA lysis buffer. The beads were lastly washed with PBS two times
570 and submitted to the Indiana University School of Medicine Proteomics Core facility for LC/MS-
571 MS.

572 **Phylogenetic analysis**

573 The DYRKs used in the phylogenetic analysis including HSDYRK1A (Q13627), HSDYRK1B
574 (Q9Y463), HSDYRK2 (Q92630), HSDYRK3 (O43781), HSDYRK4 (Q9NR20), ATDYRK1
575 (AT3G177500, ATDYRK2A (AT1G73460), ATDYRK2B (AT1G73450), ATDYRK3 (AT2G40120),

576 TGDYRK1 (TGGT1_204280) and TGDYRK2 (TGGT1_283480). The sequence alignment was
577 performed using the MUSCLE online service, the conserved regions used for tree construction
578 were extracted by using Gblocks 0.91b, and the phylogenetic tree was constructed with a
579 maximum-likelihood method by using PhyML 3.0 with the LG model. The bootstrap values
580 shown on the phylogenetic tree were obtained by repeating the generation of the phylogenetic
581 tree 100 times.

582 **Phosphoproteomics analysis**

583 Sample preparation, mass spectrometry analysis, bioinformatics, and data evaluation were
584 performed in collaboration with the Center for Proteome Analysis at the Indiana University
585 School of Medicine. Methods described below are adaptations from literature reports [56] and
586 vendor-provided protocols.

587 Fifteen samples (Experiment 1: n=3 control, IAA 6h; Experiment 2: n=3 control, IAA 1 h, and
588 IAA 3 h) submitted to the Center for Proteome Analysis were denatured in 8 M urea (CHEBI:
589 16199), 100 mM Tris-HCl, pH 8.5 (CHEBI: 975446756, Sigma-Aldrich Cat No: 10812846001)
590 with sonication using a Bioruptor® sonication system (Diagenode Inc. USA, North America cat
591 number B01020001) with 30 sec/30 sec on/off cycles for 15 minutes in a water bath at 4 °C.
592 After subsequent centrifugation at 14,000g for 20 min, protein concentrations were determined
593 by Bradford protein assay (BioRad Cat No: 5000006). Approximately 2 mg equivalent of protein
594 from each sample was then reduced with 5 mM tris(2-carboxyethyl)phosphine hydrochloride
595 (TCEP, Sigma-Aldrich Cat No: C4706) for 30 minutes at room temperature and alkylated with
596 10 mM chloroacetamide (CAA, Sigma Aldrich Cat No: C0267) for 30 min at room temperature in
597 the dark. Samples were diluted with 50 mM Tris.HCl, pH 8.5 to a final urea concentration of 2 M
598 for Trypsin/Lys-C based overnight protein digestion at 37 °C (40 µg of protein used for global
599 proteomics and the remainder for phosphoproteomics, 1:70 protease: substrate ratio, Mass
600 Spectrometry grade, Promega Corporation, Cat No: V5072.) Digestions were acidified with

601 trifluoroacetic acid (TFA, 0.5% v/v) and desalted on Sep-Pak® Vac cartridges (50 mg size for
602 global and 100 mg size for phosphopeptides Waters™ Cat No: WAT054955) with a wash of 1
603 mL 0.1% TFA followed by elution in 70% acetonitrile 0.1% formic acid (FA). Peptide
604 concentrations were checked by Pierce Quantitative colorimetric assay (Cat No: 23275) and
605 confirmed to be consistent.

606 For phosphoproteomics, each peptide sample (approximately 2 mg) was applied to a Pierce
607 High-Select™ TiO₂ Phosphopeptide Enrichment Kit (Thermo Fisher Scientific, Cat No: A32993).
608 After preparing spin tips as per the manufacturer's instructions, each sample was applied to an
609 individual enrichment tip, washed, and eluted as per the manufacturer's instructions. The
610 phosphopeptide elution was immediately dried. Global peptides and phosphopeptides were
611 each labeled with Tandem Mass Tag (TMT) reagent (manufacturer's instructions, 0.3 mg per
612 global sample and 0.5 mg per phosphopeptide sample Thermo Fisher Scientific, TMT™ Isobaric
613 Label Reagent Set; Cat No: 90111 Lot XE342654, see Table X below) for two hours at room
614 temperature, quenched with a final concentration v/v of 0.3% hydroxylamine at room
615 temperature for 15 minutes. Labeled peptides were then mixed and dried by speed vacuum.

616 For high pH basic fractionation, peptides were reconstituted in 0.1% trifluoroacetic acid and
617 fractionated on Sep-Pak® Vac cartridges using methodology and reagents from Pierce™ High
618 pH reversed-phase peptide fractionation kit (8 fractions for global proteomics and 4 for
619 phosphoproteomics skipping every other; Thermo Fisher Cat No: 84868). Samples were run
620 (1/8th of each global and 1/5th of each phosphopeptide fraction) on an EASY-nLC 1200 HPLC
621 system (SCR: 014993, Thermo Fisher Scientific) coupled to Lumos Orbitrap™ mass
622 spectrometer (Thermo Fisher Scientific.) Peptides were separated on a 25 cm EasySpray™
623 C18 column (2 μm, 100 Å, 75 μm x 25 cm, Thermo Scientific Cat No: ES902A) at 400 nL/min
624 with a gradient of 4-30% with mobile phase B (Mobile phases A: 0.1% FA, water; B: 0.1% FA,
625 80% Acetonitrile (Thermo Fisher Scientific Cat No: LS122500)) over 160 minutes, 30-80% B

626 over 10 mins; and dropping from 80-10% B over the final 10 min. The mass spectrometer was
627 operated in positive ion mode with a 4 sec cycle time data-dependent acquisition method with
628 advanced peak determination and Easy-IC (internal calibrant) on. Precursor scans (m/z 375-
629 1600) were done with an orbitrap resolution of 120000, RF lens% 30, maximum inject time 105
630 ms, AGC target of 100% (4e5), MS2 intensity threshold of 2.5e4, MIPS mode, precursor filter of
631 70% and 0.7 window, including charges of 2 to 7 for fragmentation with 30-sec dynamic
632 exclusion. MS2 scans were performed with a quadrupole isolation window of 0.7 m/z, 37% HCD
633 CE, 50000 resolution, 200% normalized AGC target (1e5), maximum IT of 86 ms, and fixed first
634 mass of 100 m/z.

635 Raw files were analyzed in Proteome Discover™ 2.5 (Thermo Fisher Scientific) with a
636 database containing *Toxoplasma gondii* GT1 proteins, UniProt reference *Homo sapiens*
637 proteome, plus common contaminants (Total sequences: 79215). Global and
638 phosphoproteomics SEQUEST HT searches were conducted with a maximum number of 3
639 missed cleavages, precursor mass tolerance of 10 ppm, and a fragment mass tolerance of 0.02
640 Da. Static modifications used for the search were 1) carbamidomethylation on cysteine (C)
641 residues; 2) TMT label on lysine (K) residues. Dynamic modifications used for the search were
642 TMT label on N-termini of peptides, oxidation of methionines, phosphorylation on serine,
643 threonine or tyrosine, deamidation of asparagine and glutamine, and acetylation, methionine
644 loss or acetylation with methionine loss on protein N-termini. Percolator False Discovery Rate
645 was set to a strict setting of 0.01 and a relaxed setting of 0.05. IMP-pm-RS node was used for
646 all modification site localization scores. Values from both unique and razor peptides were used
647 for quantification. In the consensus workflows, peptides were normalized by total peptide
648 amount with no scaling. Quantification methods utilized isotopic impurity levels available from
649 Thermo Fisher Scientific. Reporter ion quantification was allowed with an S/N threshold of 5 and
650 a co-isolation threshold of 30%. The resulting grouped abundance values for each sample type,

651 abundance ratio (AR) values, and respective p-values (ANOVA) from Proteome Discover™
652 were exported to Microsoft Excel.

653

654 **Acknowledgment**

655 We thank Drs. Peter Bradley, Marc-Jan Gubbels, and Michael Reese for sharing anti-IMC6,
656 IMC3, and *Toxoplasma*-specific anti-acetylated tubulin antibodies, respectively. We extend our
657 gratitude to Dr. Elena Suvorova for her invaluable suggestions for the project. Mass
658 spectrometry was performed by the Indiana University School of Medicine Center for Proteome
659 Analysis. Acquisition of the IUSM Proteomics instrumentation used for this project was provided
660 by the Indiana University Precision Health Initiative. This research was supported by the
661 National Institutes of Health grants R01AI149766, R01DK124067, and R21AI164619 to G.A.
662 The proteomics work was supported, in part, by the Indiana Clinical and Translational Sciences
663 Institute (UL1TR002529) and the Cancer Center Support Grant for the IU Simon
664 Comprehensive Cancer Center (P30CA082709).

665

666 **Author Contributions**

667 Chunlin Yang and Gustavo Arrizabalaga conceived and designed the experiments. Emma H.
668 Doud performed phosphoproteomics analysis. Emily Sampson performed endogenous tagging
669 of PPKL. All other experiments and data analysis were performed by Chunlin Yang. The paper
670 was written by Chunlin Yang and Gustavo Arrizabalaga. Emma H. Doud contributed to the
671 manuscript by writing the methods used for phosphoproteomic analysis.

672

673 **Competing Interests**

674 The authors declare no competing interests.

675 **References**

- 676 1. Cova, M.M., M.H. Lamarque, and M. Lebrun, *How Apicomplexa Parasites Secrete and*
677 *Build Their Invasion Machinery*. Annu Rev Microbiol, 2022. **76**: p. 619-640.
- 678 2. Striepen, B., *The apicoplast: a red alga in human parasites*. Essays Biochem, 2011. **51**:
679 p. 111-25.
- 680 3. Jeninga, M.D., J.E. Quinn, and M. Petter, *ApiAP2 Transcription Factors in Apicomplexan*
681 *Parasites*. Pathogens, 2019. **8**(2).
- 682 4. Shortt, E., et al., *CDPK2A and CDPK1 form a signaling module upstream of Toxoplasma*
683 *motility*. bioRxiv, 2022: p. 2022.07.19.500742.
- 684 5. Billker, O., S. Lourido, and L.D. Sibley, *Calcium-dependent signaling and kinases in*
685 *apicomplexan parasites*. Cell Host Microbe, 2009. **5**(6): p. 612-22.
- 686 6. Blackman, M.J. and V.B. Carruthers, *Recent insights into apicomplexan parasite egress*
687 *provide new views to a kill*. Curr Opin Microbiol, 2013. **16**(4): p. 459-64.
- 688 7. Gaji, R.Y., et al., *Phosphorylation of a Myosin Motor by TgCDPK3 Facilitates Rapid*
689 *Initiation of Motility during Toxoplasma gondii egress*. PLoS Pathog, 2015. **11**(11): p.
690 e1005268.
- 691 8. Yang, C. and G. Arrizabalaga, *The serine/threonine phosphatases of apicomplexan*
692 *parasites*. Mol Microbiol, 2017. **106**(1): p. 1-21.
- 693 9. Maselli, G.A., et al., *Revisiting the evolutionary history and roles of protein phosphatases*
694 *with Kelch-like domains in plants*. Plant Physiol, 2014. **164**(3): p. 1527-41.
- 695 10. Kim, E.J. and E. Russinova, *Brassinosteroid signalling*. Curr Biol, 2020. **30**(7): p. R294-
696 R298.
- 697 11. Zhu, J.Y., J. Sae-Seaw, and Z.Y. Wang, *Brassinosteroid signalling*. Development, 2013.
698 **140**(8): p. 1615-20.

- 699 12. Clouse, S.D., M. Langford, and T.C. McMorris, *A brassinosteroid-insensitive mutant in*
700 *Arabidopsis thaliana exhibits multiple defects in growth and development*. Plant Physiol,
701 1996. **111**(3): p. 671-8.
- 702 13. Li, J. and J. Chory, *A putative leucine-rich repeat receptor kinase involved in*
703 *brassinosteroid signal transduction*. Cell, 1997. **90**(5): p. 929-38.
- 704 14. Nam, K.H. and J. Li, *BRI1/BAK1, a receptor kinase pair mediating brassinosteroid*
705 *signaling*. Cell, 2002. **110**(2): p. 203-12.
- 706 15. Wang, X. and J. Chory, *Brassinosteroids regulate dissociation of BKI1, a negative*
707 *regulator of BRI1 signaling, from the plasma membrane*. Science, 2006. **313**(5790): p.
708 1118-22.
- 709 16. Wang, Z.Y., et al., *The brassinosteroid signal transduction pathway*. Cell Res, 2006.
710 **16**(5): p. 427-34.
- 711 17. Clouse, S.D., *Brassinosteroid signal transduction: from receptor kinase activation to*
712 *transcriptional networks regulating plant development*. Plant Cell, 2011. **23**(4): p. 1219-
713 30.
- 714 18. Mora-Garcia, S., et al., *Nuclear protein phosphatases with Kelch-repeat domains*
715 *modulate the response to brassinosteroids in Arabidopsis*. Genes Dev, 2004. **18**(4): p.
716 448-60.
- 717 19. Vert, G., et al., *Molecular mechanisms of steroid hormone signaling in plants*. Annu Rev
718 Cell Dev Biol, 2005. **21**: p. 177-201.
- 719 20. Li, J., et al., *BIN2, a new brassinosteroid-insensitive locus in Arabidopsis*. Plant Physiol,
720 2001. **127**(1): p. 14-22.
- 721 21. Wang, Z.Y., et al., *Nuclear-localized BZR1 mediates brassinosteroid-induced growth and*
722 *feedback suppression of brassinosteroid biosynthesis*. Dev Cell, 2002. **2**(4): p. 505-13.
- 723 22. Yin, Y., et al., *BES1 accumulates in the nucleus in response to brassinosteroids to*
724 *regulate gene expression and promote stem elongation*. Cell, 2002. **109**(2): p. 181-91.

- 725 23. He, J.X., et al., *The GSK3-like kinase BIN2 phosphorylates and destabilizes BZR1, a*
726 *positive regulator of the brassinosteroid signaling pathway in Arabidopsis*. Proc Natl
727 Acad Sci U S A, 2002. **99**(15): p. 10185-90.
- 728 24. Vert, G. and J. Chory, *Downstream nuclear events in brassinosteroid signalling*. Nature,
729 2006. **441**(7089): p. 96-100.
- 730 25. Guttery, D.S., et al., *A unique protein phosphatase with kelch-like domains (PPKL) in*
731 *Plasmodium modulates ookinete differentiation, motility and invasion*. PLoS Pathog,
732 2012. **8**(9): p. e1002948.
- 733 26. Back, P.S., et al., *IMC29 Plays an Important Role in Toxoplasma Endodyogeny and*
734 *Reveals New Components of the Daughter-Enriched IMC Proteome*. mBio, 2023. **14**(1):
735 p. e0304222.
- 736 27. Khan, K. and W. Khan, *Congenital toxoplasmosis: An overview of the neurological and*
737 *ocular manifestations*. Parasitol Int, 2018. **67**(6): p. 715-721.
- 738 28. Alday, P.H. and J.S. Doggett, *Drugs in development for toxoplasmosis: advances,*
739 *challenges, and current status*. Drug Des Devel Ther, 2017. **11**: p. 273-293.
- 740 29. Joyce, B.R., et al., *Phosphorylation of eukaryotic initiation factor-2alpha promotes the*
741 *extracellular survival of obligate intracellular parasite Toxoplasma gondii*. Proc Natl Acad
742 Sci U S A, 2010. **107**(40): p. 17200-5.
- 743 30. Oliveira Souza, R.O., et al., *IMC10 and LMF1 mediate mitochondrial morphology*
744 *through mitochondrion-pellicle contact sites in Toxoplasma gondii*. J Cell Sci, 2022.
745 **135**(22).
- 746 31. Liffner, B. and S. Absalon, *Expansion Microscopy Reveals Plasmodium falciparum*
747 *Blood-Stage Parasites Undergo Anaphase with A Chromatin Bridge in the Absence of*
748 *Mini-Chromosome Maintenance Complex Binding Protein*. Microorganisms, 2021. **9**(11).
- 749 32. Sidik, S.M., et al., *A Genome-wide CRISPR Screen in Toxoplasma Identifies Essential*
750 *Apicomplexan Genes*. Cell, 2016. **166**(6): p. 1423-1435 e12.

- 751 33. Brown, K.M., S. Long, and L.D. Sibley, *Conditional Knockdown of Proteins Using Auxin-*
752 *inducible Degron (AID) Fusions in Toxoplasma gondii*. Bio Protoc, 2018. **8**(4).
- 753 34. Francia, M.E. and B. Striepen, *Cell division in apicomplexan parasites*. Nat Rev
754 Microbiol, 2014. **12**(2): p. 125-36.
- 755 35. Chen, C.T. and M.J. Gubbels, *The Toxoplasma gondii centrosome is the platform for*
756 *internal daughter budding as revealed by a Nek1 kinase mutant*. J Cell Sci, 2013. **126**(Pt
757 15): p. 3344-55.
- 758 36. Suvorova, E.S., et al., *A novel bipartite centrosome coordinates the apicomplexan cell*
759 *cycle*. PLoS Biol, 2015. **13**(3): p. e1002093.
- 760 37. Branon, T.C., et al., *Efficient proximity labeling in living cells and organisms with TurboID*.
761 Nat Biotechnol, 2018. **36**(9): p. 880-887.
- 762 38. Soppa, U. and W. Becker, *DYRK protein kinases*. Curr Biol, 2015. **25**(12): p. R488-9.
- 763 39. Gaji, R.Y., A.K. Sharp, and A.M. Brown, *Protein kinases in Toxoplasma gondii*. Int J
764 Parasitol, 2021. **51**(6): p. 415-429.
- 765 40. Tran, J.Q., et al., *SPM1 stabilizes subpellicular microtubules in Toxoplasma gondii*.
766 Eukaryot Cell, 2012. **11**(2): p. 206-16.
- 767 41. Wang, X., et al., *Cryo-EM structure of cortical microtubules from human parasite*
768 *Toxoplasma gondii identifies their microtubule inner proteins*. Nat Commun, 2021. **12**(1):
769 p. 3065.
- 770 42. Alvarez, C.A. and E.S. Suvorova, *Checkpoints of apicomplexan cell division identified in*
771 *Toxoplasma gondii*. PLoS Pathog, 2017. **13**(7): p. e1006483.
- 772 43. Anderson-White, B., et al., *Cytoskeleton assembly in Toxoplasma gondii cell division*. Int
773 Rev Cell Mol Biol, 2012. **298**: p. 1-31.
- 774 44. Torres, J.A., et al., *Identification and Molecular Dissection of IMC32, a Conserved*
775 *Toxoplasma Inner Membrane Complex Protein That Is Essential for Parasite Replication*.
776 mBio, 2021. **12**(1).

- 777 45. Anderson-White, B.R., et al., *A family of intermediate filament-like proteins is*
778 *sequentially assembled into the cytoskeleton of Toxoplasma gondii*. Cell Microbiol, 2011.
779 **13**(1): p. 18-31.
- 780 46. Beck, J.R., et al., *A novel family of Toxoplasma IMC proteins displays a hierarchical*
781 *organization and functions in coordinating parasite division*. PLoS Pathog, 2010. **6**(9): p.
782 e1001094.
- 783 47. Baptista, C.G., et al., *Toxoplasma F-box protein 1 is required for daughter cell scaffold*
784 *function during parasite replication*. PLoS Pathog, 2019. **15**(7): p. e1007946.
- 785 48. Back, P.S., et al., *Multivalent Interactions Drive the Toxoplasma AC9:AC10:ERK7*
786 *Complex To Concentrate ERK7 in the Apical Cap*. mBio, 2021. **13**(1): p. e0286421.
- 787 49. Malumbres, M., *Cyclin-dependent kinases*. Genome Biol, 2014. **15**(6): p. 122.
- 788 50. Liu, J., et al., *Novel thioredoxin-like proteins are components of a protein complex*
789 *coating the cortical microtubules of Toxoplasma gondii*. Eukaryot Cell, 2013. **12**(12): p.
790 1588-99.
- 791 51. Engelberg, K., et al., *Proteomic characterization of the Toxoplasma gondii cytokinesis*
792 *machinery portrays an expanded hierarchy of its assembly and function*. Nat Commun,
793 2022. **13**(1): p. 4644.
- 794 52. Yang, C., et al., *A plasma membrane localized protein phosphatase in Toxoplasma*
795 *gondii, PPM5C, regulates attachment to host cells*. Sci Rep, 2019. **9**(1): p. 5924.
- 796 53. Huynh, M.H. and V.B. Carruthers, *Tagging of endogenous genes in a Toxoplasma*
797 *gondii strain lacking Ku80*. Eukaryot Cell, 2009. **8**(4): p. 530-9.
- 798 54. Yang, C., W.J. Blakely, and G. Arrizabalaga, *The Tyrosine Phosphatase PRL Regulates*
799 *Attachment of Toxoplasma gondii to Host Cells and Is Essential for Virulence*. mSphere,
800 2022. **7**(3): p. e0005222.
- 801 55. Dos Santos Pacheco, N., et al., *Revisiting the Role of Toxoplasma gondii ERK7 in the*
802 *Maintenance and Stability of the Apical Complex*. mBio, 2021. **12**(5): p. e0205721.

803 56. Grecco, G.G., et al., *A multi-omic analysis of the dorsal striatum in an animal model of*
804 *divergent genetic risk for alcohol use disorder*. *J Neurochem*, 2021. **157**(4): p. 1013-
805 1031.

806

807

808 **Figure Legends**

809 **Figure 1. PPKL shows dynamic localization during division.** A. Schematic of PPKL in
810 *Toxoplasma*. B, C, D, and E. Intracellular parasites of the PPKL^{HA} strain were stained with anti-
811 HA antibodies to monitor PPKL localization in non-dividing parasites (B) and in parasites in the
812 mid (C), late (D), or early (E) stages of division. Division was monitored with antibodies against
813 IMC3 (B-E) or Centrin1 (E). The white arrow in E indicates the area expanded in the box. Scale
814 bar: 5 μ m.

815 **Figure 2. Ultrastructural expansion microscopy reveals PPKL in basal and apical**
816 **structures.** Intracellular and extracellular parasites were fixed with paraformaldehyde,
817 expanded in acrylamide gels, and stained with NHS-ester, anti-HA, and anti-acetylated tubulin.
818 Images were captured by LSM 900 with Airyscan. A. Image of intracellular non-dividing
819 parasites. The white box frames the region expanded to the right of the arrow. B. Images of
820 intracellular dividing parasites. C, D. Images of extracellular parasites. The white framed zone in
821 D is zoomed in and shown in the lower right corner. E. Image of intracellular parasites. The
822 parasite on the right has started daughter parasite assembly, as shown by duplicated
823 centrosomes, preconoidal regions, and the apical polar rings, which are framed in a black box.
824 The box is enlarged to the left showing the acetylated tubulin signal, and to the right showing
825 both anti-acetylated tubulin and anti-HA. F. Image shows intracellular parasites in a late stage of
826 division.

827 **Figure 3. Depletion of PPKL leads to disruption of parasite division.** A. Shown is
828 representative Western blot of protein extract of the AID-tagged PPKL strain (PPKL^{AID}) treated
829 with auxin (IAA) for times indicated and probed for the HA epitope tag. The protein Sag1 was
830 used as a loading control. B and C. Parasites from the parental (par) or PPKL^{AID} were grown for
831 6 days in the absence or presence of auxin (IAA) and allowed to form plaques. B shows
832 representative plaque assays. The graph in C is the average plaque area formed by the two

833 strains, based on data collected from four biological replicates, with three experimental
834 replicates for each. For each biological replicate, the data was normalized to the average plaque
835 area of the parental strain without IAA treatment. The error bars represent standard deviations.
836 ^{***}, $P < 0.001$; n.s., no significance (Student's t-test, two tails, unequal variance). D to F. PPKL^{AID}
837 parasites were grown with/without auxin for 18 hours (D and E) or 42 hours (F) and analyzed by
838 IFA. The cultures were stained with anti-acetylated tubulin, anti-IMC3, and Dapl. Scale bar: 5
839 μm .

840 **Figure 4. Depletion of PPKL does not affect the replication of centrosomes.** Centrosome
841 duplication of PPKL^{AID} grown with and without auxin was monitored by IFA using antibodies
842 against centrin1. A. IFA of parasites grown with/without IAA for 18 hours and stained with anti-
843 IMC3, anti-Centrin1 antibodies, and Dapl. B. IFA of PPKL^{AID} parasites grown with/without IAA
844 for 6 hours. C. quantification of dividing PPKL^{AID} parasites treated with/without IAA for 6 hours
845 with one or two daughters. Three biological replicates were performed, with 50 parasites
846 counted for each replicate. The error bars represent standard deviations. D. U-ExM of one
847 daughter containing PPKL^{AID} parasite treated with IAA for 6 hours and stained with anti-
848 acetylated tubulin, anti-Centrin1, NHS-ester, and Draq5. Scale bar: 5 μm .

849 **Figure 5. Depletion of PPKL reduces the rigidity of microtubules.** The cortical cytoskeleton
850 was extracted from PPKL^{AID} parasites treated with IAA or ethanol for 6 hours. A. IFA of the
851 extracted cortical cytoskeleton used anti-acetylated tubulin and anti-IMC6 antibodies to monitor
852 the microtubules and IMC, respectively. Examples of fragmented microtubule are indicated by
853 white arrows. B. Quantification of fragmented microtubules normalized to the number of cortical
854 cytoskeletons. The bars indicate the average number of fragment microtubules from each
855 cortical cytoskeleton. The error bars represent standard deviations. Three biological replicates,
856 each consisting of two experimental replicates, were performed. For each experimental replicate,

857 10 random fields of view were selected to count the number of cortical cytoskeleton and
858 fragmented microtubules. **, $P < 0.01$ (Student's t-test, two tails, unequal variance).

859 **Figure 6. DYRK1 is a plant-like kinase and plays an important role in parasite division. A.**

860 Phylogenetic analysis of DYRK sequences from humans (HSDYRK1A, 1B, 2, 3, and 4),
861 *Arabidopsis* (ATDYRK1, 2A, 2B, and 3), and *Toxoplasma* (TGDYRK1 and 2). DYRKs from
862 *Toxoplasma* are highlighted. Alignment and tree construction details and accession numbers
863 are listed in the Methods session. B. IFA of parasites expressing Myc-tagged DYRK1 using anti-
864 Myc and anti-IMC6 antibodies. The upper panel shows non-dividing parasites, while the lower
865 panel shows dividing ones. Scale bar: 5 μm . C. The diagram depicts the CRISPR/Cas9-
866 mediated strategy used to disrupt the *DYRK1* gene. P1, 2, 3, and 4 are the three amplicons
867 used to confirm the integration of the DHFR cassette between the Cas9 cutting sites and the
868 deletion of the *DYRK1* gene. D. Agarose gel of PCR products amplified from the genomic DNA
869 extracted from Δ *DYRK1* parasites using the four sets of primers indicated in C. The P1 amplicon
870 has a length of 2928 bp in the Δ *DYRK1* genome and 4787 bp in the parental genome. The P2,
871 P3, and P4 amplicons have a length of 339 bp, 431 bp, and 196 bp, respectively. E and F.
872 Δ *DYRK1* and parental strain parasites were allowed to form plaques in culture for six days. A
873 representative plaque assay (E) and the quantification are shown (F). The bars represent the
874 relative average plaque areas. Three biological replicates were performed, and six experimental
875 replicates were included each time. For each biological replicate, the data was normalized to the
876 average plaque area of the parental. G. IFA images of Δ *DYRK1* parasites that show abnormal
877 division. H. Quantification of the ratio of vacuoles containing parasites displaying abnormal
878 division or morphologies. *** $P < 0.001$ (Student's t-test, two tails, unequal variance).

879 **Figure 7. Phosphoproteome analysis showed that depletion of PPKL results in increased**

880 **phosphorylation of SPM1 and decreased phosphorylation of Crk1.** A. Venn diagrams

881 showing the number of proteins with phospho-peptides that were more or less abundant in

882 PPKL^{AID} parasites treated with auxin for 1, 3 and 6 hours. The overlap indicates the number of
883 proteins that had phosphopeptides that increased and decreased in abundance upon PPKL
884 depletion. The number of proteins that were also identified as PPKL neighboring proteins in
885 each category is shown in parentheses. The fold change cutoffs are as follows: for 1 h timepoint
886 sample set, phospho-peptides with FC ≥ 1.5 and FC ≤ 0.66 , for 3 h and 6 h timepoints sample
887 sets, phospho-peptides with FC ≥ 2 and FC ≤ 0.5 . B. 3D Scatter plot shows 35 phospho-
888 peptides that are shared by all the three timepoint sample sets after filtering with the cutoffs
889 described above. Each dot in the 3D Scatter plot represents one phosphopeptide. The dots
890 shown in orange are peptides from PPKL neighboring proteins identified by TurboID analysis.
891 The dot shown in pink represents the peptide from Crk1. X-axis: the log₂ fold change of 1 h
892 samples. Y-axis: the log₂ fold change of 3 h samples. Z-axis: the log₂ fold change of 6 h
893 samples.

894 **Figure 8. A proposed functional model for PPKL.** The localization and potential function of
895 PPKL in the different stages of division (left most column) are listed in the second and third
896 columns.

897 **Figure S1. PPKL localizes to the nucleus.** A. Western blot of protein samples after
898 cytoplasmic and nuclear fractionation. Anti-HA was used to detect HA-tagged PPKL. Anti-eIF2 α
899 and anti-histoneH3 were used as controls to detect eIF2 α , a cytoplasmic protein, and histone
900 H3, a nuclear protein. B. ImageJ was used to quantify the relative intensity of the bands in the
901 two portions labeled by the same antibody. Fisher exact test was used to compare the ratios of
902 cytoplasmic/nuclear of PPKL was significantly different from that of the control eIF2 α .

903 **Figure S2. Fusion of AID to the C-terminus of PPKL reduced its expression.** A. Western
904 blot of protein samples isolated from PPKL^{HA} and PPKL^{AID} parasites. Anti-HA was used to detect
905 PPKL-3xHA and PPKL-AID-3xHA. The protein Sag1 was used as a loading control. B. The

906 quantification of the Western blot in panel A reveals the relative expression levels of PPKL-AID-
907 3xHA normalized to Sag1 and PPKL-3xHA.

908 **Figure S3. PPKL-TurboID validation.** A. Localization of PPKL-TurboID-3xHA in intracellular
909 parasites assessed by IFA. B. Western blot showing biotinylated proteins extracted from
910 PPKL^{TurboID} parasites treated with or without D-biotin. Detection was achieved using
911 Streptavidin-Conjugated Horseradish Peroxidase.

912 **Table 1. Putative PPKL neighboring proteins.** Listed are proteins identified by TurboID that
 913 met the following criteria: 1) identified in both replicates; 2) a total of 10 or more peptides
 914 identified between the two replicates; 3) fold change between experiment and control equal to or
 915 larger than 3.5. Proteins related to the IMC, Apical, Basal complex, and microtubules are
 916 highlighted with light blue; proteins related to vesicle transport were highlighted with light green;
 917 and proteins related to RNA splicing are highlighted with light orange. The number of peptides
 918 listed is the total between the two replicates.

ID	Annotation	Fold Change	Peptides		ID	Annotation	Fold Change	Peptides	
			Control	PPKL-TurboID				Control	PPKL-TurboID
244380	cactin	INF	0	363	285500	hypothetical protein	INF	0	20
293180	NADP-specific glutamate dehydrogenase	INF	0	169	237290	hypothetical protein	INF	0	20
290170	PPKL	INF	0	167	263520	SPM1	INF	0	20
245560	hypothetical protein	INF	0	151	205380	fructose-bisphosphatase	INF	0	19
232340	PPM2A	INF	0	116	213392	surface antigen repeat-containing protein	INF	0	19
313270	hypothetical protein	INF	0	103	296010	phosphatidylinositol 3- and 4-kinase	INF	0	19
269410	hypothetical protein	INF	0	102	305340	corepressor complex CRC230	INF	0	18
310220	hypothetical protein	INF	0	86	310440	MORN1	INF	0	18
203780	hypothetical protein	INF	0	86	291950	RNA recognition motif-containing protein	INF	0	18
321620	dynamamin-related protein DRPB	INF	0	84	294730	hypothetical protein	INF	0	18
243200	IMC29	INF	0	80	258540	phosphoglycerate mutase family protein	INF	0	17
291180	hypothetical protein	INF	0	70	313430	hypothetical protein; Putative nucleoporin	INF	0	17
227800	EPS15	INF	0	68	219710	hypothetical protein	INF	0	16
244120	hypothetical protein	INF	0	58	244470	RNG2	INF	0	15
220270	IMC6	INF	0	57	280370	hypothetical protein	INF	0	15
214180	EpsL	INF	0	55	260540	IMC14	INF	0	14
259640	nucleoporin autopeptidase	INF	0	54	273560	Kinesin B	INF	0	14
294360	putative ubiquitin specific protease 39 isoform 2	INF	0	51	294610	putative histone lysine methyltransferase, SET	INF	0	13
268950	hypothetical protein	INF	0	49	249440	hypothetical protein	INF	0	13
275490	hypothetical protein	INF	0	46	282070	hypothetical protein	INF	0	12
311400	SEC31A	INF	0	44	214970	putative DNA replication licensing factor	INF	0	12
212140	hypothetical protein	INF	0	40	286580	IMC17	INF	0	12
292950	AC10	INF	0	36	218960	AP2XII-1	INF	0	12
262150	K13	INF	0	33	270770	PWI domain-containing protein	INF	0	12
231070	protein kinase	INF	0	29	306660	RNA pseudouridine synthase superfamily protein	INF	0	12
221660	DEAD/DEAH box helicase domain-containing protein	INF	0	29	310950	AP2XI-3	INF	0	12
204280	DYRK1	INF	0	29	204160	GYF domain-containing protein	INF	0	11
207370	hypothetical protein	INF	0	28	212260	Sjogren's	INF	0	10

						syndrome/scleroderma autoantigen 1 (Autoantigen p27) protein			
313790	hypothetical protein	INF	0	28	270890	hypothetical protein	INF	0	10
230210	IMC10	INF	0	27	313910	RNA recognition motif 2 protein	INF	0	10
275350	TBC domain-containing protein	INF	0	25	311230	BCC7	63	2	126
265870A	pantoate-beta-alanine ligase	INF	0	25	253440	SRPK1	50	1	50
298610	GYF domain-containing protein	INF	0	24	201700	SEC13	34	1	34
320080	hypothetical protein	INF	0	24	248700	IMC12	16	1	16
235340	ISC1	INF	0	23	313380	ILP1	14	1	14
250700	hypothetical protein	INF	0	22	216000	IMC3	13	3	39
228150	hypothetical protein	INF	0	21	231640	IMC1	8.54	24	205
214880	AC4	INF	0	20	253430	putative asparagine synthetase	6.5	6	39
260580	hypothetical protein	INF	0	20	231630	IMC4	5.89	18	106
260600	TgPuf1	INF	0	20	313010	DDX6	5.75	4	23
223420	DnaJ domain-containing protein	INF	0	20	294620	putative eukaryotic initiation factor-3, subunit 8	3.5	4	14

919

920

921 **Table 2. PPKL-dependent phosphopeptides.** Listed are proteins with phosphopeptides
 922 whose numbers were either increased or decreased in PPKL^{AID} parasites treated with auxin at
 923 all time points tested (1, 3, and 6 hours). For the 3 h and 6 h timepoints sample sets,
 924 phosphopeptides with FC >= 2 and FC <= 0.5 are listed. For the 1 h timepoint sample set,
 925 phosphopeptides with FC >=1.5 and FC <= 0.66 are listed.

926

ID	Annotation	Peptides	Modification	Fold change (+IAA/-IAA)		
				1h	3h	6h
TGGT1_250830	SAC3/GANP family protein	[R].ESSKDLHAEK.[T]	1xPhospho [S]	4.37	15.87	3.737
TGGT1_263520	microtubule associated protein SPM1	[K].KLP S EEGSDYGYQKPQK.[Y]	2xPhospho [S4(100); S8(100)]	2.12	12.83	3.099
		[K].KLP S EEGSDYGYQKPQK.[Y]	1xPhospho [S4(100)]	2.43	14.78	5.256
TGGT1_235470	myosin A	[R].SSDVHAVDHSGNVYK.[G]	1xPhospho [S/Y]	1.62	10.29	7.252
TGGT1_321680	hypothetical protein	[K].EGREEEEEET A SEEEDEHAEPK.[K]	2xPhospho [T10(100); S12(100)]	2.02	9.7	21.505
TGGT1_278660	putative P-type ATPase4	[R].R FSS KRE S TVGGSGTGHSQLGK.[S]	3xPhospho [S3(100); S4(100); S8(98.7)]	1.57	5.89	4.058
TGGT1_214270	putative translation initiation factor IF-2	[R].DDSDDETKPAPPAK.[K]	1xPhospho [S/T]	1.98	2.53	2.772
		[R].RGGL SS DEEFEAK.[K]	2xPhospho [S5(100); S6(100)]	2.07	5.87	2.904
TGGT1_265250	RNA recognition motif-containing protein	[K]. SKS PDFSELRK.[E]	2xPhospho [S1(100); S3(100)]	2.11	5.7	2.629
TGGT1_209600	hypothetical protein	[K].EAQESSDDEDEDDAHFDGEDLK.[V]	1xPhospho [S]	1.87	4.51	2.718
TGGT1_289650	PEP-carboxykinase I	[R].TQSSGSLKDSISFLEMLK.[K]	2xPhospho [T/S]	1.86	4.44	2.247
TGGT1_269180	MIF4G domain-containing protein	[R].RRGS N AGAAALPAGDGK.[V]	1xPhospho [S4(100)]	1.71	3.88	6.936
TGGT1_248420	hypothetical protein	[R]. SSS VSTIFK.[M]	2xPhospho [S2(99.5); S3(100)]	2.58	2.32	3.833
TGGT1_291930	RNA recognition motif-containing protein	[K].DVMMEEESEDED S DEEKSERPVK.[K]	2xPhospho [S12(100); S18(98.8)]	0.49	0.25	0.257
		[K].NEKDVMMEEESEDED S DEEK.[S]	2xPhospho [S11(100); S15(100)]	0.61	0.09	0.312
TGGT1_288380	heat shock protein HSP90	[K].SVDKE ITE SEDEEKPAEDAEEK.[K]	2xPhospho [T7(100); S9(100)]	0.58	0.1	0.282
TGGT1_286790	nuclear factor NF2	[K].KGLSADSD S DKVSETKS.[-]	2xPhospho [S11(100); S15(98)]	0.42	0.16	0.193
		[K].KGLSADSD S DKVSETK.[S]	2xPhospho [S7(100); S11(99.2)]	0.44	0.3	0.223
		[K].KGLSADSD S DKVSETKS.[-]	3xPhospho [S7(100); S11(100); S15(97.9)]	0.53	0.15	0.136
TGGT1_209060	thrombospondin type 1 domain-containing protein	[R].EN S QENQNAEPGETHAETEEVE S NA S EKLAK.[V]	3xPhospho [S3(100); S23(98.5); S26(100)]	0.61	0.15	0.21
TGGT1_229490	tetratricopeptide repeat-containing protein	[R].NKWPGVEE ESS DDGDKEGGPSGMR.[K]	2xPhospho [S10(100); S11(100)]	0.59	0.15	0.239
TGGT1_224850	putative polyadenylate binding protein	[K].EGED S GAEEKEEEEGQKR.[E]	1xPhospho [S5(100)]	0.58	0.18	0.24
TGGT1_214270	putative translation initiation factor IF-2	[K].DD S DETKPAPPAK.[K]	1xPhospho [S3(100)]	0.66	0.18	0.313
TGGT1_244650	putative eukaryotic initiation factor-5	[K].KKAD S DD S DDDGQNGK.[E]	2xPhospho [S5(100); S9(100)]	0.39	0.2	0.206
TGGT1_310170	hypothetical protein	[R].SGVTAPGGDKDTEEL S DD S DDEAGDKDEGETNRVPGR.[D]	2xPhospho [S17(100); S21(100)]	0.64	0.21	0.289
TGGT1_204160	GYF domain-containing protein	[K].KKGD S DS E E D A S EGDLATSR.[S]	3xPhospho [S5(100); S7(100); S12(99.9)]	0.58	0.22	0.295
TGGT1_216410	hypothetical protein	[K].IVDDITADQENDE SGKS DE S DADKAESR.[E]	3xPhospho [S14(100); S17(100); S20(100)]	0.58	0.27	0.274

TGGT1_264990	hypothetical protein	[R].QEGNDKVPQSAAPSAS RQQSEENK.[R]	2xPhospho [S]	0.62	0.24	0.481
TGGT1_321520	hypothetical protein	[K].CDWDKWIDSDDEDK.[G]	1xPhospho [S9(100)]	0.61	0.26	0.222
TGGT1_228400	WD domain, G-beta repeat-containing protein	[K].NFPTPFEPKSDDDDDDE DLDELK.[S]	1xPhospho [S10(100)]	0.55	0.28	0.442
TGGT1_219150	zinc finger, zz type domain-containing protein	[R].LLEMNVGCHEEKESE DDGDKK.[R]	1xPhospho [S14(100)]	0.66	0.28	0.297
TGGT1_297170	putative 50S ribosomal protein L17	[R].RPSAAEWEEESDEEEK ADSPSPYK.[M]	2xPhospho [S10(98.5); S12(98.5)]	0.61	0.34	0.265
TGGT1_216730	MCM2/3/5 family protein	[R].AAEDAEGEEIASQLQS LDLSDGSKKK.[R]	2xPhospho [S21(99.1); S24(100)]	0.51	0.36	0.391
TGGT1_304970	cell-cycle-associated protein kinase CDK, Crk1	[R].LGSNNFDEQKHQDSF R.[F]	1xPhospho [S3(100)]	0.55	0.4	0.379
TGGT1_212770	hypothetical protein	[R].ERSDASRGPLVEALGG VDQTGADKDEK.[S]	2xPhospho [S3(100); S6(100)]	0.65	0.42	0.462

928 **Supplementary datasets**

929 **Supplementary Dataset 1.** Proteins immunoprecipitated with TgPPKL and identified by LC-
930 MS/MS. The cutoff of fold change is $PPKL.3xHA /Control \geq 2$.

931 **Supplementary Dataset 2.** List of proteins biotinylated by the PPKL-TurboID fusion. For each
932 repeat, the fold change cutoff was $PPKL-TurboID/Control \geq 2$. The list of PPKL neighboring
933 proteins was selected based on the following criteria: in combination with two replicates, 1)
934 identified in both replicates; 2) a total of 10 or more peptides were identified between the two
935 replicates; 2) the fold change was equal to or larger than 3.5.

936 **Supplementary Dataset 3.** Listed are phosphopeptides identified in PPKL^{AID} parasites treated
937 with auxin or ethanol for 6 h by phosphoproteomics analysis. The sheet "PeptideGroups"
938 contains all phospho-peptides identified in parasites and host cells. *Toxoplasma*
939 phosphopeptides that were significantly ($p\text{-value} \leq 0.05$) increased or decreased in auxin-
940 treated parasites are listed in the sheets titled "Toxo Increased" and "Toxo Decreased". The
941 phosphopeptides that were increased or decreased by more than two-fold in phosphorylation
942 are listed in "6h Increased FC >2" and "6h Decreased FC < 0.5". The phosphopeptides that
943 were from the proteins identified by TurboID analysis are listed in "Increase overlap with
944 TurboID" and "Decrease overlap with TurboID". Proteins in Fig. 8A have been listed in the sheet
945 "Proteins of Fig. 8A". Those proteins that are PPKL neighboring proteins identified by TurboID
946 analysis were highlighted.

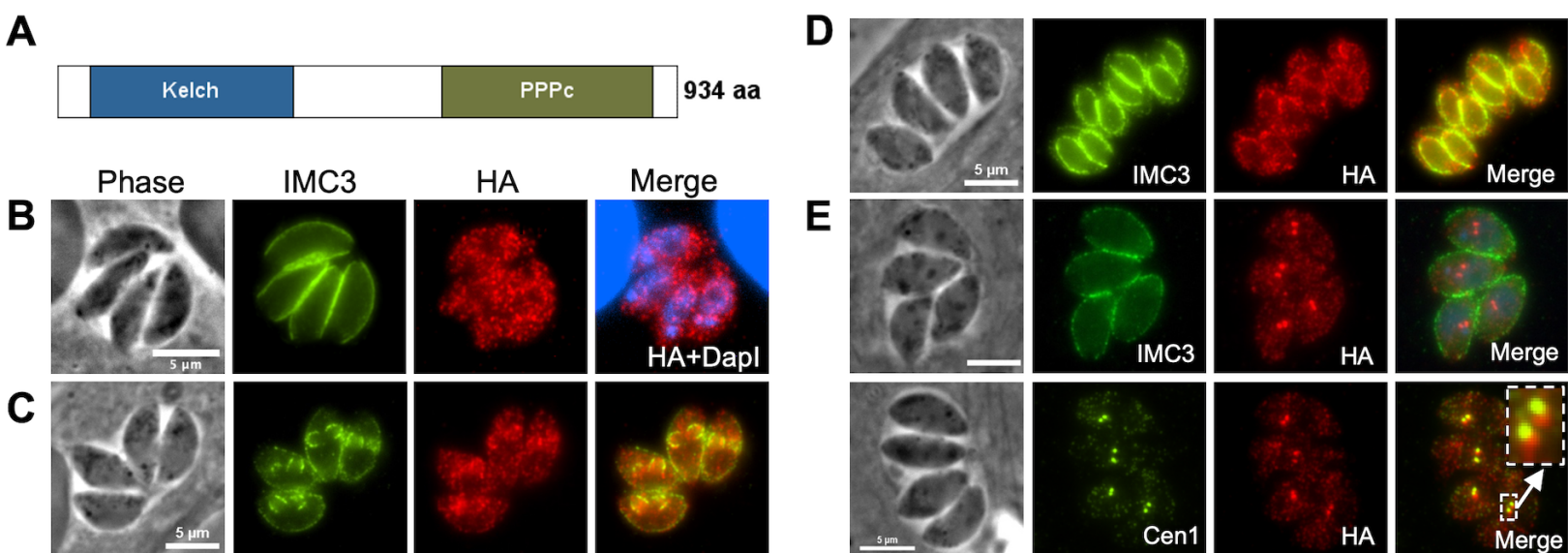
947 **Supplementary Dataset 4.** Listed are phosphopeptides identified in PPKL^{AID} parasites treated
948 with auxin for 1 and 3 h or ethanol for 1 h. The sheet 'PeptideGroups' lists all phosphopeptides
949 identified in parasites and host cells. The phosphopeptides identified in parasites are shown in
950 the sheet "Toxo peptides". The phosphopeptides that are more/less abundant in 1 or 3 h auxin-
951 treated parasites were filtered via specific fold changes and are shown in corresponding sheets.

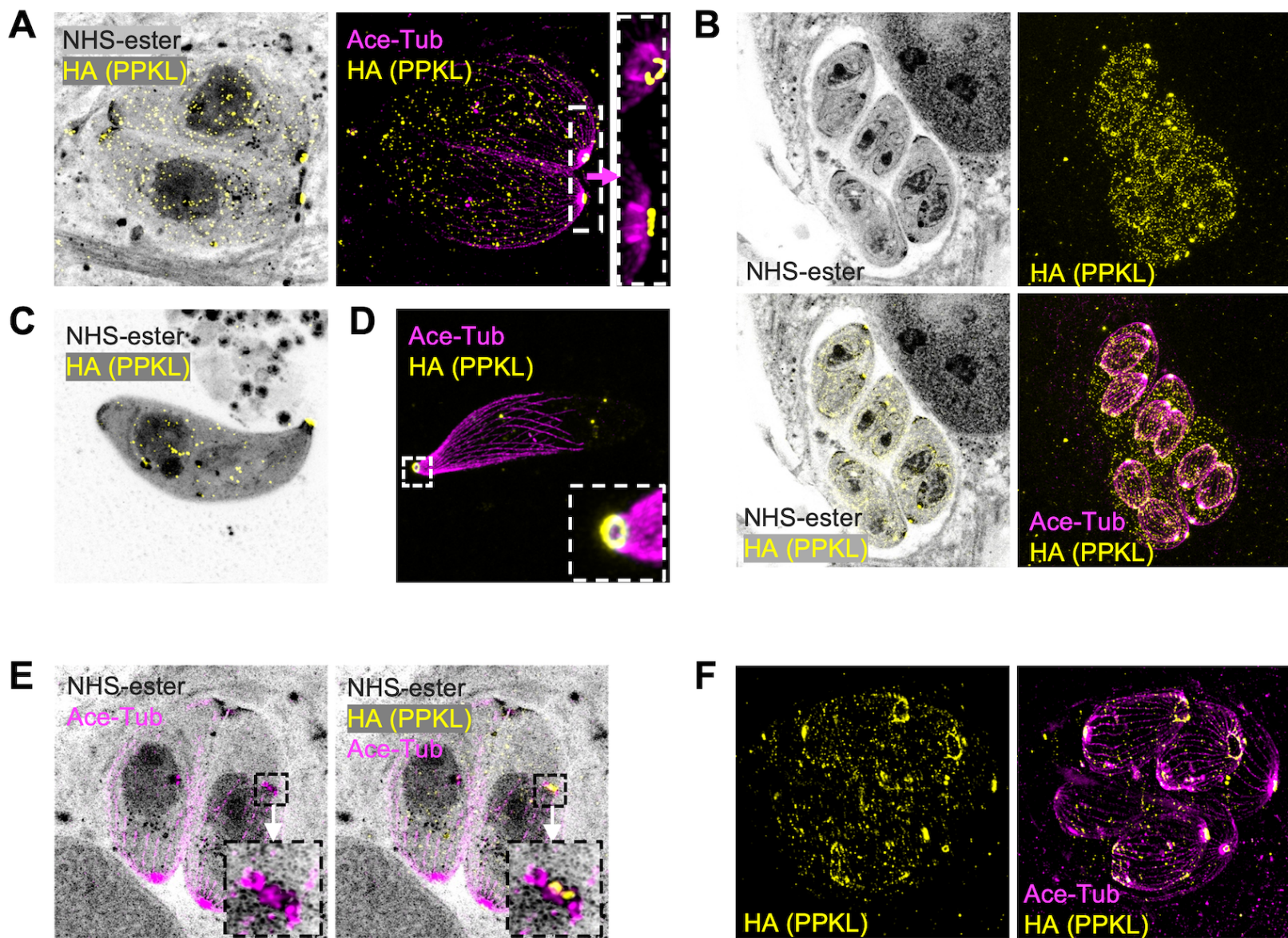
952 Proteins of Fig. 8A have listed in the sheet "Proteins of Fig. 8A". Proteins identified as putative

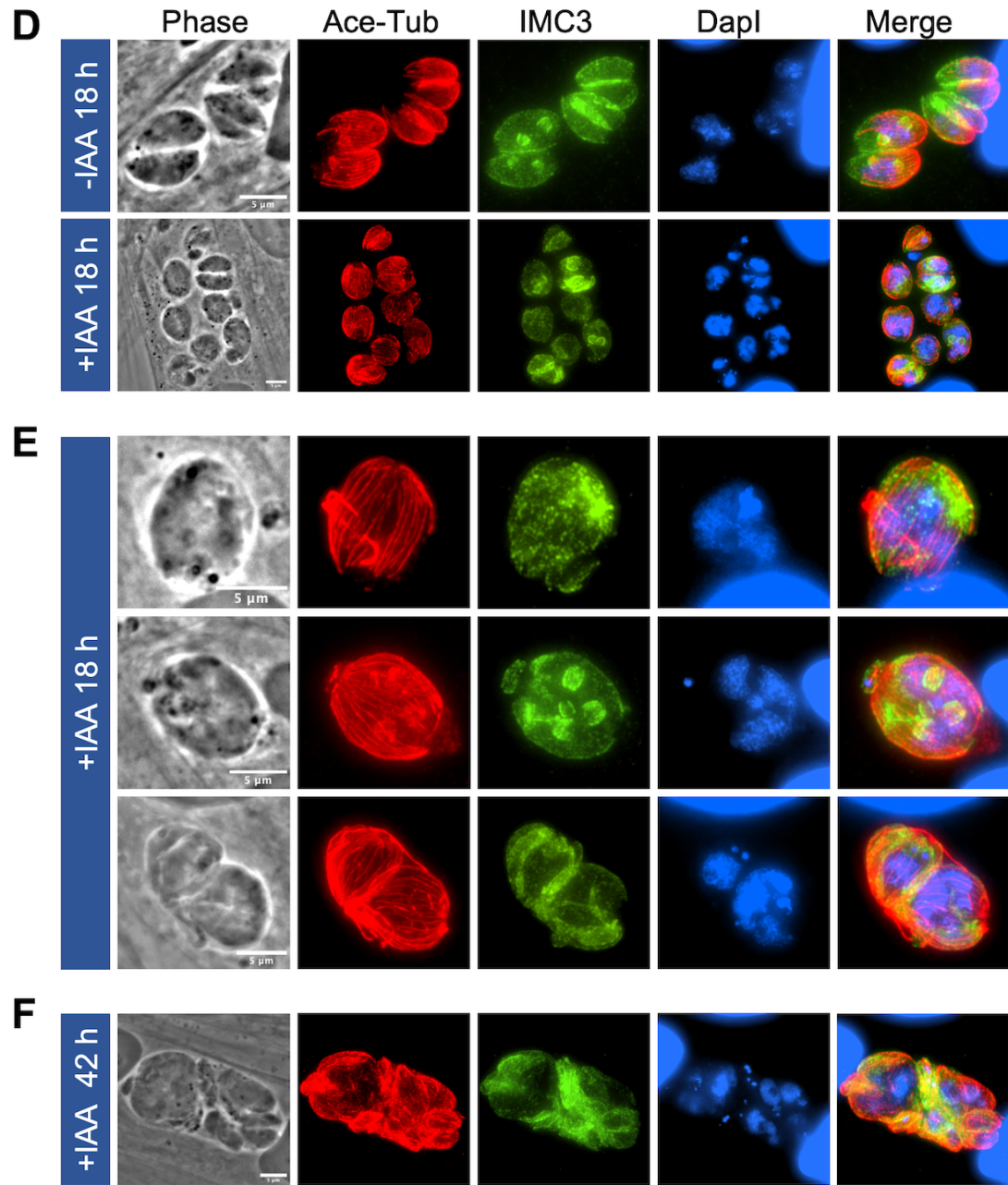
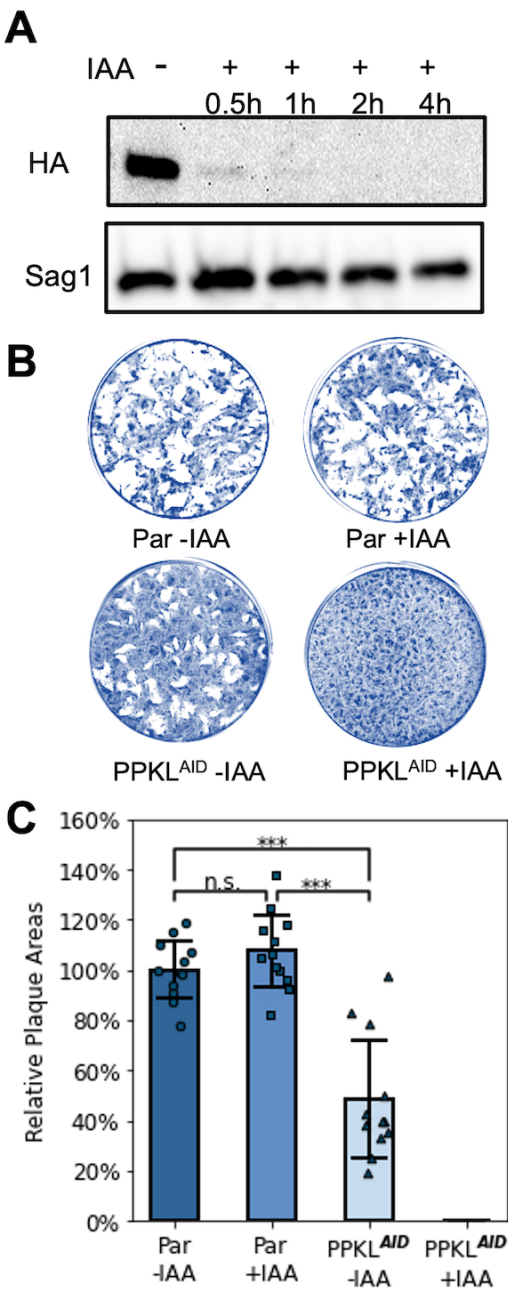
953 PPKL neighboring proteins by TurboID are highlighted.

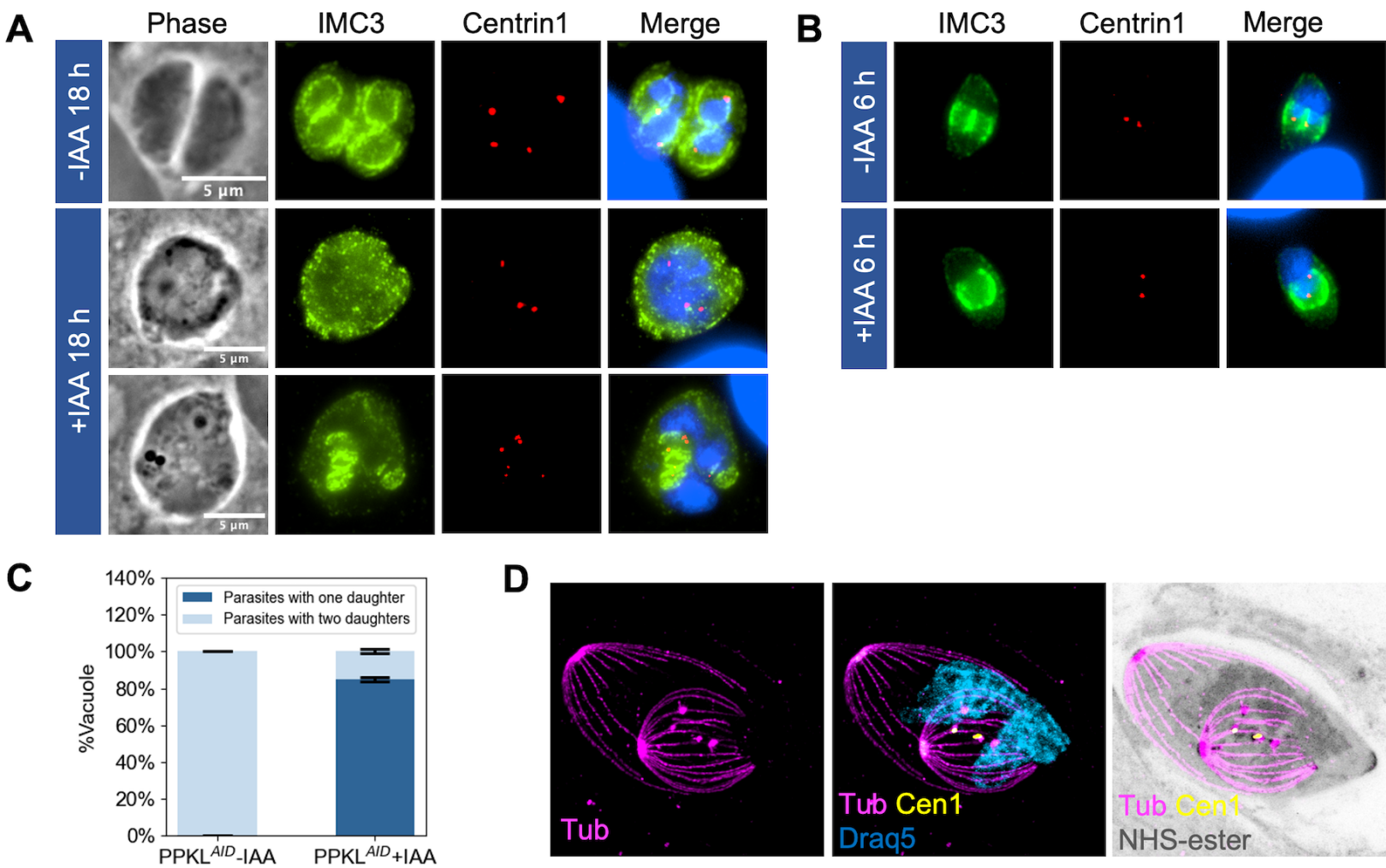
954 **Supplementary Dataset 5.** List of primers used in this study.

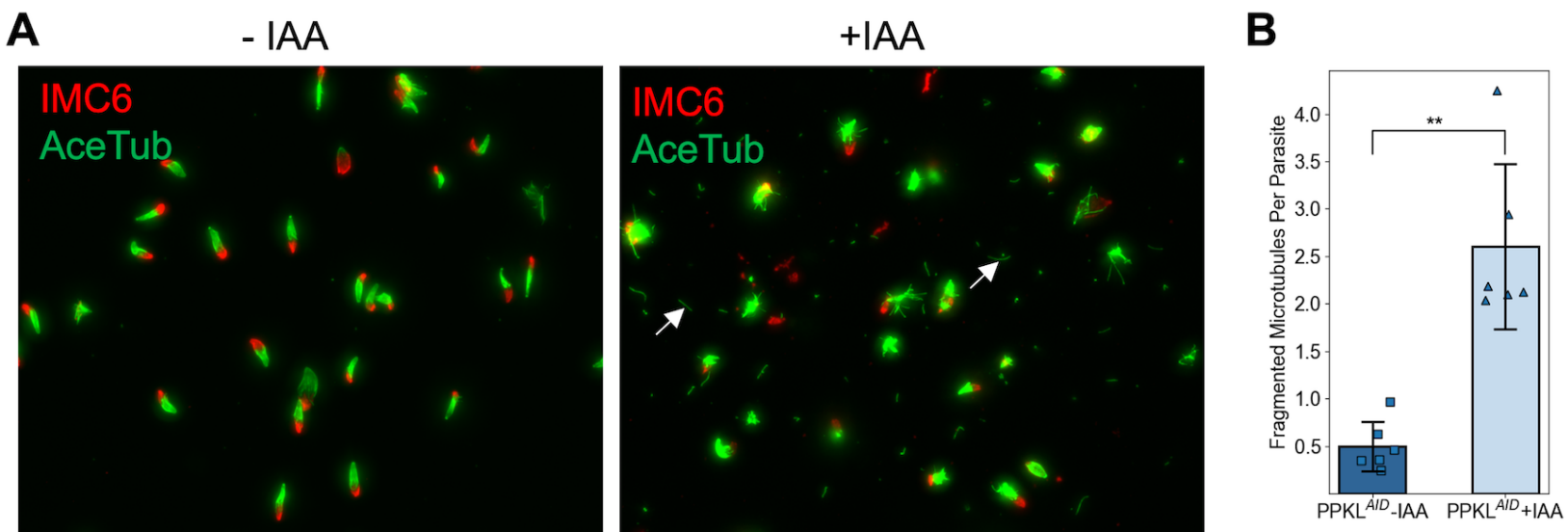
955

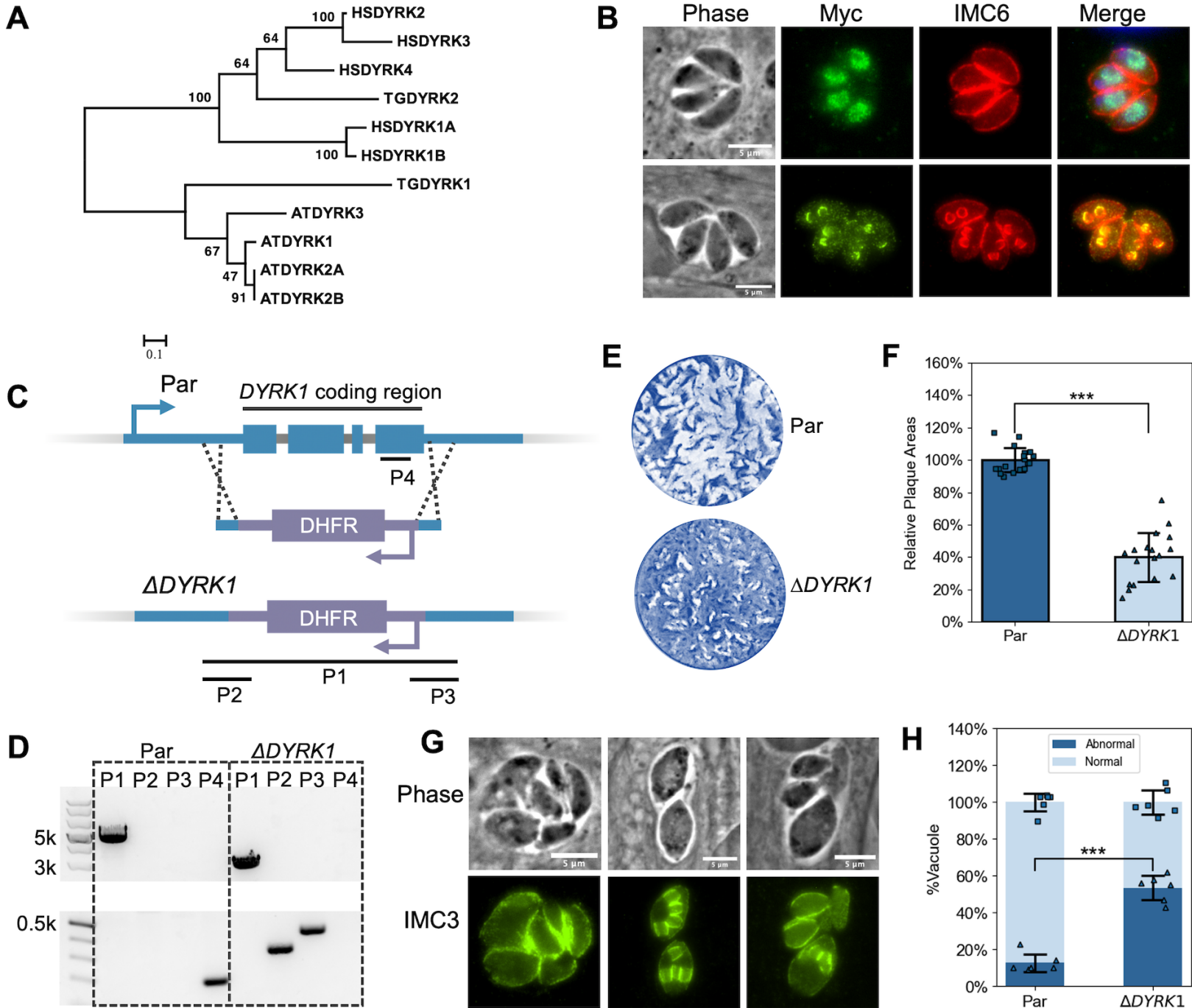




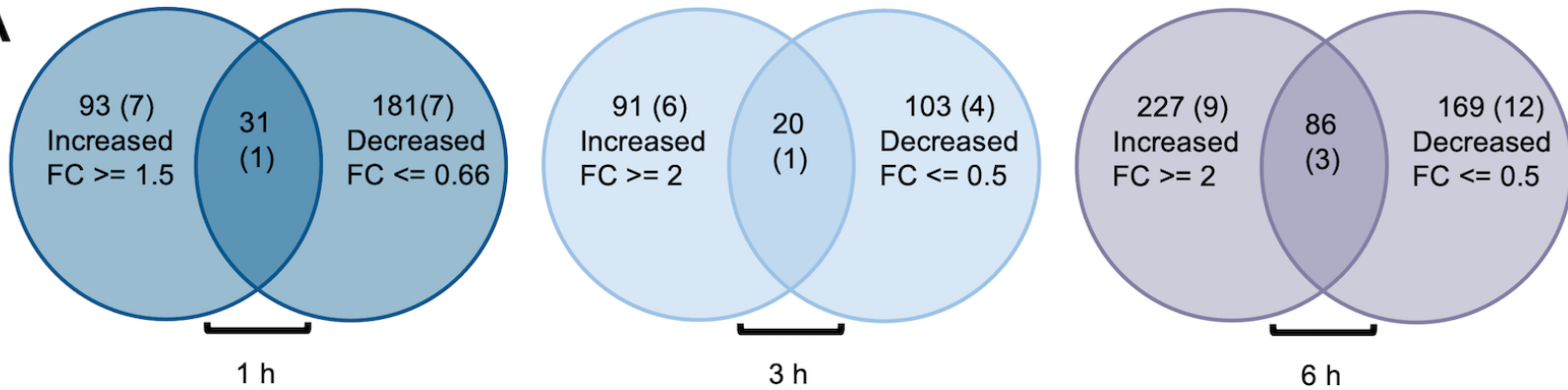




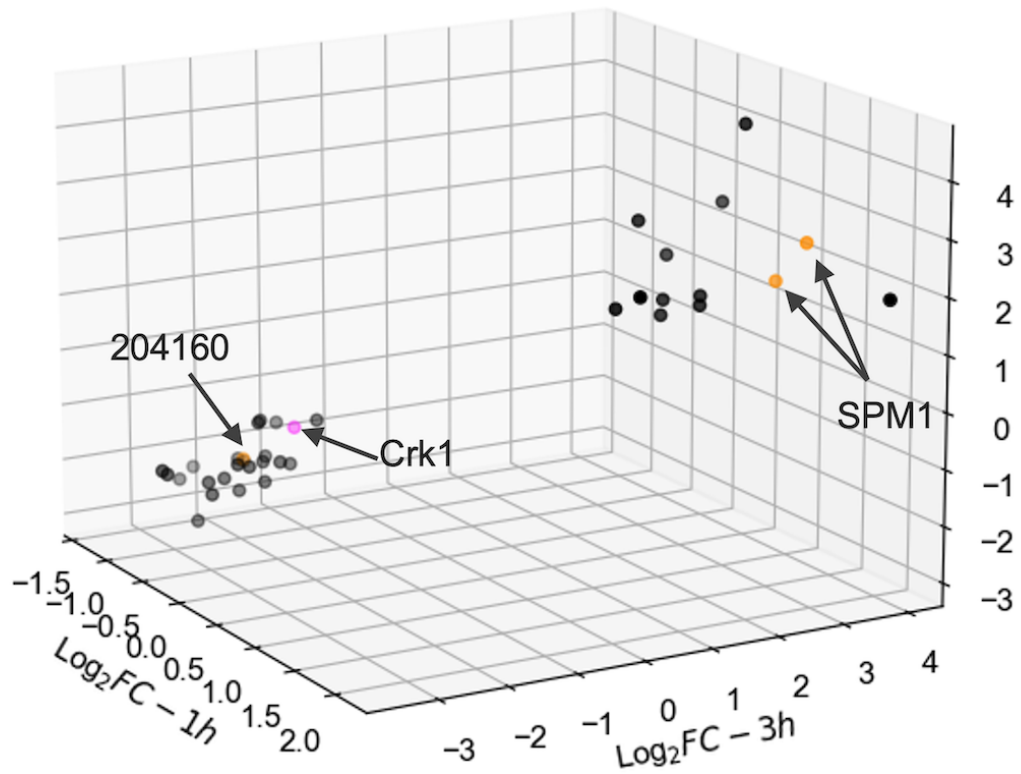




A



B



		PPKL	
		Localization	Potential Function
Parasite division	Before Division	Cytosol/Nucleus	It may regulate a pathway that activates Crk1 and potentially involves DYRK1.
	Initiation	Preconoidal region	Unknown
	Early Stage	Daughter parasite cortical cytoskeleton	It regulates microtubule rigidity and compact structure, potentially by mediating the phosphorylation status of SPM1.
	Mid Stage		
	Late Stage	Basal complex ring	It may terminate microtubule extension.